the EGF-induced migration of A431 cells by inhibiting H-Ras farnesylation.

CONFLICT OF INTEREST

The authors declare no conflict of interest.

ACKNOWLEDGEMENTS

We would like to thank MicroBiopharm Japan Co., Ltd. (formerly Mercian Corp.) for kind gift of ACM. This study was supported by KAKENHI (60200854), and the SCADS was supported by a Grant-in-Aid for Scientific Research on Priority Area 'Cancer' from The Ministry of Education, Culture, Sports, Science and Technology, Japan.

1 Gupta, G. P. & Massagué, J. Cancer metastasis: building a framework. *Cell* **127,** 679–695 (2006).
2 Fox, P. L., Sa, G., Dobrowolski, S. F. & Stacey, D. W. The regulation of endothelial cell motility by p21 ras. *Oncogene* **9,** 3519–3526 (1994).
3 Ridley, A. J., Comoglio, P. M. & Hall, A. Regulation of scatter factor/hepatocyte growth factor responses by Ras, Rac and Rho in MDCK cells. *Mol. Cell Biol.* **15,** 1110–1122 (1995).
4 Rowinsky, E. K., Windle, J. J. & Hoff Von, D. D. Ras protein farnesyltransferase: a strategic target for anticancer therapeutic development. *J. Clin. Oncol.* **17,** 3631–3652 (1999).
5 Takemoto, Y. *et al.* Chemistry and biology of moverastins, inhibitors of cancer cell migration, produced by *Aspergillus*. *Chem. Biol.* **12,** 1337–1347 (2005).
6 Oki, T., Matsuzawa, Y., Yoshimoto, A., Numata, K. & Kitamura, I. New antitumor antibiotics aclacinomycins A and B. *J. Antibiot.* **28,** 830–834 (1975).
7 Hori, S. *et al.* Antitumor activity of new anthracycline antibiotics, aclacinomycin-A and its analogs, and their toxicity. *Jpn. J. Cancer Res.* **68,** 685–690 (1977).
8 Sekizawa, R. *et al.* Isolation of novel saquayamycins as inhibitors of farnesyl-protein transferase. *J. Antibiot.* **49,** 487–490 (1996).
9 Kwon, B.-M. *et al.* Farnesyl protein transferase inhibitory components of polygonum multiflorum. *Arch. Pharm. Res.* **32,** 495–499 (2009).
10 Sawada, M. *et al.* Synthesis and anti-migrative evaluation of moverastin derivatives. *Bioorg. Med. Chem. Lett.* **21,** 1385–1389 (2011).
11 Engelman, J. A. Targeting PI3K signalling in cancer: opportunities, challenges and limitations. *Nat. Rev. Cancer* **9,** 550–562 (2009).
12 Rodriguez-Viciana, P., Warne, P. H., Vanhaesebroeck, B., Waterfield, M. D. & Downward, J. Activation of phosphoinositide 3-kinase by interaction with Ras and by point mutation. *EMBO J.* **15,** 2442–2451 (1996).

Supplementary Information accompanies the paper on The Journal of Antibiotics website (http://www.nature.com/ja)

ORGANIC LETTERS
2012
Vol. 14, No. 17
4418–4421

Synthesis and Assignment of the Absolute Configuration of Indenotryptoline Bisindole Alkaloid BE-54017

Tomoyuki Kimura,[†] Shuhei Kanagaki,[‡] Yusuke Matsui,[‡] Masaya Imoto,[‡] Takumi Watanabe,*[,†] and Masakatsu Shibasaki*[,†]

Institute of Microbial Chemistry, Tokyo, 3-14-23 Kamiosaki, Shinagawa-ku, Tokyo 141-0021, Japan, and Faculty of Science and Technology, Department of Biosciences and Informatics, Keio University, Yokohama, 223-8522, Japan

twatanabe@bikaken.or.jp; mshibasa@bikaken.or.jp

Received July 12, 2012

ABSTRACT

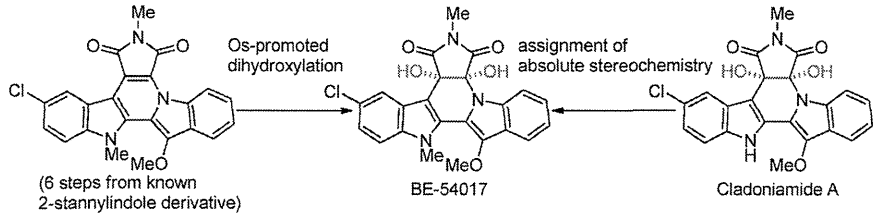

Synthesis of the indenotryptoline bisindole alkaloid, BE-54017, was accomplished using osmium-promoted *cis*-dihydroxylation of maleimide as a key step. After optical resolution, the absolute configuration of this molecule was determined by comparing its optical rotation and HPLC profile to those obtained for BE-54017 derived from enantiopure cladoniamide A, whose stereochemistry has been reported previously. BE-54017 with the correct absolute stereochemistry induced apoptosis of epidermal growth factor (EGF)-stimulated EGF receptor overexpressing A431 cells and inhibited vacuolar-type H^+-ATPase (V-ATPase).

The bisindole alkaloid family of natural products is a rich source of bioactive substances,[1,2] including potential lead compounds of medicines for clinical use. Among them, indolocarbazole-type compounds,[3] represented by rebeccamycin (**3**)[4] and staurosporine (**4**),[5] occur widely in nature. Typically, the carbon at the 3-position of each indole subunit connects to a characteristic five-membered ring heterocycle such as maleimide or γ-lactam. Less commonly observed, however, is another subfamily of bisindole alkaloids, the indenotryotoline-type compounds, in which one of the indole subunits of the indolocarbazole scaffold is flipped so that the nitrogen atom at the 1-position forms a bond with the 5-membered heterocycle, creating an asymmetrical overall framework (Figure 1). BE-54017 (**1**), an indenotryptoline-type bisindole alkaloid, was first reported as a natural cytotoxic product (i.e., IC_{50} for P388: 0.11 μg/mL) isolated from *Streptomyces* sp. A54017 by the Banyu group in 2000.[6] A recent study to screen for selective inducers of epidermal growth factor (EGF)-dependent apoptosis in EGF receptor (EGFR)-overexpressing tumor cells revealed that BE-54017 exhibited the desired activity. Overexpression of EGFR is observed in many tumor types and seems to enhance tumor development and malignancy; therefore, the development of EGFR-targeting drugs has been anticipated for their therapeutic efficiency.[7] In fact, BE-54017 dose-dependently induced apoptosis in EGF-stimulated A431 cells that overexpress EGFR, but not in other types of human tumor cells that do not overexpress the EGFR. Because of the unusual structure and biological

[†] Institute of Microbial Chemistry, Tokyo.
[‡] Keio University.

(1) Ryan, K. S.; Drennan, C. L. *Chem. Biol.* **2009**, *16*, 351.
(2) Higuchi, K.; Kawasaki, T. *Nat. Prod. Rep.* **2007**, *24*, 843.
(3) Nakano, H.; Omura, S. *J. Antibiot.* **2009**, *62*, 17.
(4) (a) Nettleton, D. E.; Doyle, T. W.; Krishnan, B.; Matsumoto, G. K.; Clardy, J. *Tetrahedron Lett.* **1985**, *26*, 4011. (b) Bush, J. A.; Long, B. H.; Catino, J. J.; Bradner, W. T.; Tomita, K. *J. Antibiot.* **1987**, *40*, 668.
(5) (a) Omura, S.; Iwai, Y.; Hirano, A.; Nakagawa, A.; Awaya, J.; Tsuchiya, H.; Takahashi, Y.; Masuma, R. *J. Antibiot.* **1977**, *30*, 275. (b) Rüegg, U. T.; Burgess, G. M. *Trends Pharmacol. Sci.* **1989**, *10*, 218.
(6) Nakase, K.; Nakajima, S.; Hirayama, M.; Kondo, H.; Kojiri, K.; Suda, H. JP 2000178274, 2000.
(7) Martini, M.; Vecchione, L.; Siena, S.; Tejpar, S.; Bardelli, A. *Nat. Rev. Clin. Oncol.* **2012**, *9*, 87.

10.1021/ol3019314
Published on Web 08/23/2012

activity of BE-54017, synthetic studies were performed to assign its relative and absolute configurations.

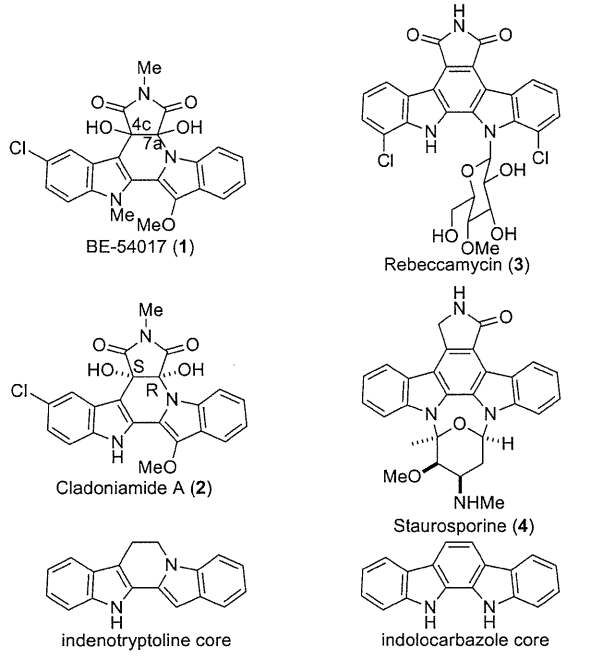

Figure 1. Structure of BE-54017 and related bisindole alkaloids.

In 2008, Davies and Andersen reported the isolation and structure determination of cladoniamide A (**2**), a desmethyl homologue of BE-54017, produced by *Streptomyces* uncialis.[8] In that study, the absolute stereochemistry of cladoniamide A was unequivocally assigned as shown in Figure 1 by X-ray crystallographic analysis; vicinal *cis*-diol in the 4c and 7a positions has the *S*- and *R*-configuration, respectively. Moreover, Chang and Brady recently proposed the biosynthetic pathway of BE-54017.[9] According to their report, the three methyltransferases (ie., Abe M1, Abe M2, and Abe M3) are responsible for the stepwise introduction of the three methyl groups at the late stage of the biosynthesis, which implies that cladoniamide A is a possible biosynthetic precursor of BE-54017. Although no stereochemical information on BE-54017 itself has been provided to date, it is likely that the diol moiety of this molecule also has a *cis* orientation and its absolute configuration should thus be 4c*S*,7a*R*. Herein, we report the first synthesis of indenotryptoline bisindole alkaloide BE-54017 and determination of the absolute stereochemistry of this molecule using the synthetic approach.

Scheme 1 depicts the synthetic design of BE-54017 in the present study. Because of the rarity of the indenotryptoline scaffold, only scattered reports describing synthetic efforts on structurally related compounds are found in the literature. The vicinal *cis*-diol was anticipated to be introduced

Scheme 1. Structure of BE-5417 and Related Bisindole Alkaloids

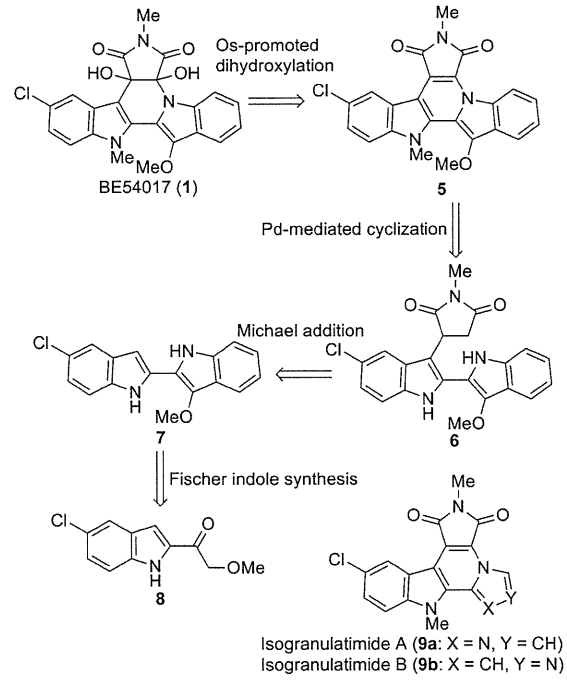

at the final stage of the synthesis by metal-mediated dihydroxylation of an unreactive double bond embedded in the maleimide moiety of **5**. This intermediate contains the entire hexacyclic system of BE-54017, which was planned to be constructed by the Michael addition of a bisindole **7** to maleimide, affording **6**, followed by Pd-promoted cyclization and subsequent methylation. This two-step protocol for the C–C and C–N bond formation was inspired by precedents in which a similar reaction sequence was examined with maleimide and indolylimidazoles or indolylpyrroles as the substrate in an effort to synthesize the analogues[10] of isogranulatimides A and B (**9a** and **9b**, respectively).[11] The bisindole building block **7** should be prepared by Fischer indole synthesis using properly functionalized 2-acylindole **8**.

Scheme 2. Model Study on Dihydroxylation of Maleimide Using an Isogranulatimide Analogue

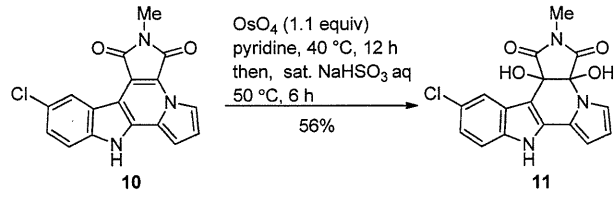

Prior to our attempt to synthesize BE-54017, the conditions for *cis*-dihydroxylation of the maleimide moiety were

(8) Williams, D. E.; Davies, J.; Patrick, B. O.; Bottriell, H.; Tarling, T.; Roberge, M.; Andersen, R. J. *Org. Lett.* **2008**, *10*, 3501.

(9) (a) Chang, F. -Y.; Brady, S. F. *J. Am. Chem. Soc.* **2011**, *133*, 9996. (b) Ryan, K. S. *PLoS One* **2011**, *6*, e23694.

(10) (a) Hugon, B.; Pfeiffer, B.; Renard, P.; Prudhomme, M. *Tetrahedron Lett.* **2003**, *44*, 3927. (b) Hugon, B.; Anizon, F.; Bailly, C.; Golsteyn, R. M.; Pierré, A.; Léonce, S.; Hickman, J.; Pfeiffer, B.; Prudhomme, M. *Bioorg. Med. Chem.* **2007**, *15*, 5965.

screened using a structurally simplified substrate **10** that can be prepared according to the reported procedure.[10] The standard conditions with a catalytic amount of OsO_4 in the presence of NMO as a co-oxidant did not work, and all of the starting material was recovered. This result is consistent with the previous report that dihydroxylation of *N*-phenylmaleimide under identical conditions resulted in an extremely low yield (4%).[12] No reaction occurred when the *N*-methylated congener of **10** was used. Addition of citric acid to the media showed no improvement in efficacy of the reaction.[13] Ru- and Mn-based oxidation was also not effective for this system, and no reaction took place ($RuCl_3$ (0.5 or 2.5 mol %), $NaIO_4$ (1.4 or 1.5 equiv), $CeCl_3$ (10 mol %), 0 °C for 18 h,[14] and $Mn(ClO_4)_2 \cdot 6H_2O$ (0.3 mol %), pyridine-2-COOH (1.8 mol %), NaOAc (3.0 mol %), H_2O_2, (2.0 equiv), 0 °C to rt for 18 h,[15] respectively). We then returned to osmium-mediated reactions and discovered that the reaction proceeded with reasonable efficacy when a stoichiometric amount of OsO_4 (1.1 equiv) was used, giving rise to the osmate ester of **10**, which could be converted to the free form using a reductive workup procedure (saturated aq $NaHSO_3$, 50 °C for 6 h) in 56% yield (Scheme 2). Encouraged by this result, we began the synthesis of BE-54017 as shown in Scheme 3.

Scheme 3. Synthetic Route to BE-54017 (**1**)

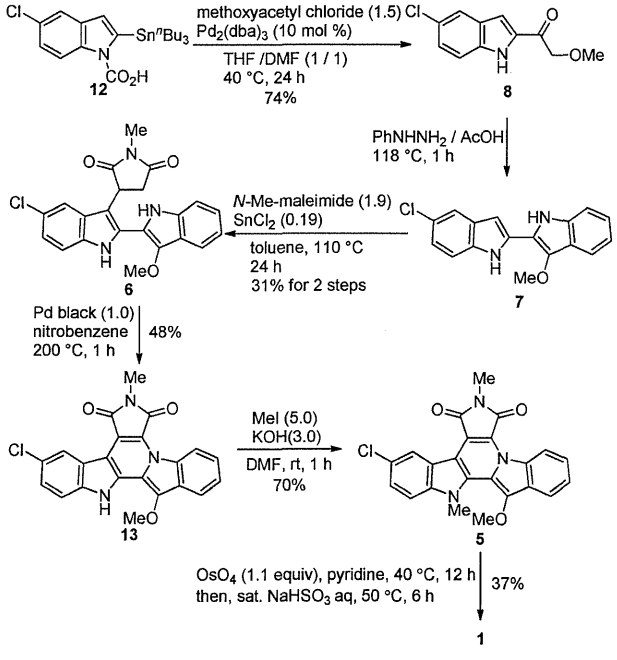

Synthesis commenced with Stille coupling between the known stannane **12**[16] and 1.2 equiv of methoxyacetyl chloride to afford **8**. The use of 10 mol % of $(Ph_3P)_2PdCl_2$ resulted in a poor yield even under reflux in toluene (4%). Changing the palladium source to 10 mol % of $Pd_2(dba)_3$ along with switching the solvent to THF or DMF slightly improved the yield even at ambient temperatures (11% and 16%, respectively). A mixed solvent system of equal volumes of THF and DMF dramatically increased the chemical yield to 46%. Finally, slightly increasing the reaction temperature to 40 °C afforded the desired coupling product in 74% yield. Upon reflux at 80 °C, however, decomposition of the stannane **12** predominated.

In the next step, the 2-acylindole derivative **8** was subjected to the standard Fischer indole synthesis protocol in the presence of phenylhydrazine to afford unstable bisindole intermediate **7**, which was immediately used without purification for the succeeding Michael addition to maleimide to give **6** in 31% over two steps. The cyclization of **6** was accomplished by treating a stoichiometric amount of Pd black in nitrobenzene under heating at 200 °C[10] leading to **13** in moderate yield (48%), and the whole BE-54017 framework was constructed at this stage. Subsequent methylation of the indenotryptoline intermediate **13** with excess MeI in the presence of 3.0 equiv of KOH as a base afforded **5** in 70% yield. The prolonged reaction time in this step resulted in opening the maleimide core, which substantially reduced the isolated yield. Finally, OsO_4-promoted dihydroxylation and a subsequent reductive workup as demonstrated in the model study completed the synthesis of BE-54017 (37%). All of the physicochemical data of the synthetic sample except for optical rotation were indistinguishable from those of the natural product.[6]

Synthetic BE-54017 was submitted to an optical resolution to define its absolute stereochemistry and elucidate a relationship between its stereochemistry and biological activity. To this end, an HPLC method using a chiral stationary phase (Daicel, CHIRALPAC IC 4.6 × 250 mm, 20% AcOEt in *n*-hexane, 2 mL/min) was effective. Two enantiomers were eluted at retention times of 8.0 and 10.0 min: the first enantiomer had a negative specific rotation value ($[\alpha]^{24}_D$ −347 (c = 0.075, DMSO)), whereas the second enantiomer had a positive specific rotation value ($[\alpha]^{24}_D$ +332 (c = 0.065, DMSO)). The value of the first enantiomer was consistent with the reported value for BE-54017 ($[\alpha]^{20}_D$ −428 (c = 0.5, DMSO)). With enantiopure BE-54017 in hand, the stage was set for determination of its absolute configuration. Toward this end, BE-54017 was independently prepared starting from enantiopure cladoniamide A whose absolute stereochemistry is known.[8]

The reaction sequence shown in Scheme 3 could be also applied to the synthesis of cladoniamide A (**2**). In fact, the intermediate with the complete framework, **13**, was transformed into racemic cladoniamide A under the

(11) (a) Berlinck, R. G. S.; Britton, R.; Piers, E.; Lim, L.; Roberge, M.; da Rocha, R. M.; Andersen, R. J. *J. Org. Chem.* **1998**, *63*, 9850. (b) Roberge, M.; Berlinck, R. G. S.; Xu, L.; Anderson, H. J.; Lim, L. Y.; Curman, D.; Stringer, C. M.; Friend, S. H.; Davies, P.; Vincent, I.; Haggarty, S. J.; Kelly, M. T.; Britton, R.; Piers, E.; Andersen, R. J. *Cancer Res.* **1998**, *58*, 5701.

(12) Bromba, C.; Carrie, P.; Chui, J. K. W.; Flyes, T. M. *Supramol. Chem.* **2009**, *21*, 81.

(13) Éll, A. H.; Closson, A.; Adolfsson, H.; Bäckvall, J.-E. *Adv. Synth. Catal.* **2003**, *345*, 1012.

(14) Plietker, B.; Niggemann, M. *J. Org. Chem.* **2005**, *70*, 2402.

(15) Saisaha, P.; Pijper, D.; van Summeren, R. P.; Hoen, R.; Smit, C.; de Boer, J. W.; Hage, R.; Alsters, P. L.; Feringa, B. L.; Browne, W. R. *Org. Biomol. Chem.* **2010**, *8*, 4444.

(16) Hudkins, R. L.; Diebold, J. L.; Marsh, F. D. *J. Org. Chem.* **1995**, *60*, 6218.

Scheme 4. Determination of the Absolute Stereochemistry of BE-54017 (**1**)

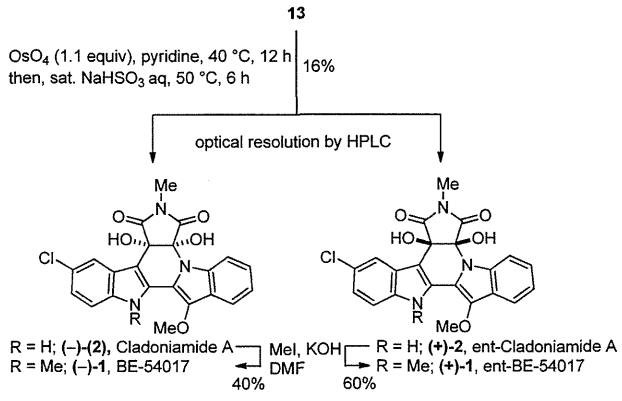

dihydroxylation conditions (Scheme 4). All of the physicochemical data other than optical rotation obtained from the synthetic cladoniamide A were confirmed to be identical to those of the natural sample. To our delight, the succeeding optical resolution could be accomplished uneventfully by HPLC under the same protocol used for the separation of BE-54017 (Daicel, CHIRALPAC IC 4.6 × 250 mm, 20% AcOEt in *n*-hexane, 2 mL/min). The fraction eluted out at 8.3 min showed a specific rotation of $[\alpha]^{22}_{D}$ −256 (c = 0.080, MeOH) that is consistent with the reported optical rotation for natural cladoniamide A ($[\alpha]^{22.5}_{D}$ −390.0 (c = 1.88, MeOH)).[8] This enantiomer (cladoniamide A, (−)-**2**) was subjected to *N*-methylation with MeI and KOH to give BE-54017 ((−)-**1**), confirming that the absolute configuration of the vicinal diols of BE-54017 was 4c*S*,7a*R*. Independently, the other enantiomer of cladoniamide A ((+)-**2**) was converted to (+)-**1** *ent*-BE-54017 using the same *N*-methylation procedure.

Each enantiomer was subjected to an assay to evaluate EGF-dependent apoptosis of human epidermal carcinoma A431 cells (see the Supporting Information). Synthetic BE-54017 ((−)-**1**) induced EGF-dependent apoptosis in a dose-dependent manner with an EC_{50} value of 0.16 μg/mL, consistent with that of natural BE-54017 (EC_{50} value of 0.23 μg/mL). In contrast, the antipode ((+)-**1**) was more than 10 times less potent (EC_{50} > 3.0 μg/mL). The results indicated that the stereochemistry of the diol moiety has a critical role in the observed capabililty to intervene in the EGF-mediated signaling pathway. The difference in biological activity supports the accuracy of the assignment of the absolute stereochemistry.

We previously reported that vacuolar-type H^+-ATPase (V-ATPase) inhibitors, such as concanamycin B and destruxin E, exhibited inhibitory activity toward EGF-mediated signaling pathways.[17] Therefore, we next examined whether BE54017 inhibited V-ATPase. BE-54017 inhibited the acidification of acidic organelles maintained by V-ATPases, indicating that BE-54017 induced EGF-dependent apoptosis in EGFR-overexpressing A431 cells, possibly through inhibiting V-ATPase activity (see the Supporting Information).

In summary, we synthesized BE-54017, a rare member of the indenotryptoline subfamily of bisindole alkaloid natural products, using osmium-promoted dihydroxylation of the maleimide core as the key step. After optical resolution of the synthetic sample by HPLC, the absolute configuration of BE-54017 was identified as 4c*S*,7a*R* by comparison of its specific rotation and HPLC profile to those obtained from independently prepared BE-54017 derived from enantiopure cladoniamide A, whose stereochemistry was reported previously. Further studies of the structure–activity relationship of the compounds in this class are underway.

Acknowledgment. We are grateful to Dr. R. Sawa and Ms. Y. Kubota for HRMS and NMR analysis and to Dr. M. Igarashi for preparation of natural BE-54017.

Supporting Information Available. Experimental procedures, detail in biological study, and spectroscopic data for new compounds. This material is available free of charge via the Internet at http://pubs.acs.org.

(17) (a) Yoshimoto, Y.; Imoto, M. *Exp. Cell Res.* **2002**, *279*, 118. (b) Yoshimoto, Y.; Jyojima, T.; Arita, T.; Ueda, M.; Imoto, M.; Matsumura, S.; Toshima, K. *Bioorg. Med. Chem. Lett.* **2002**, *12*, 3525.

The authors declare no competing financial interest.

SCIENTIFIC REPORTS

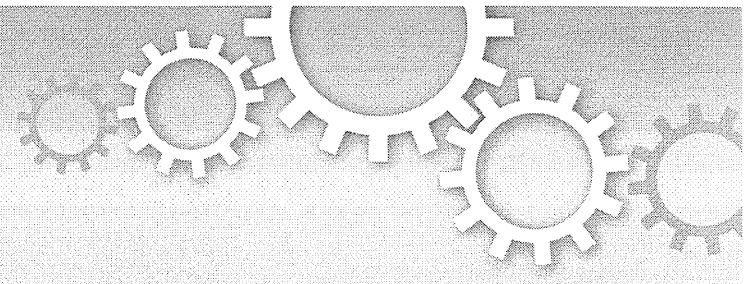

OPEN

SUBJECT AREAS:
CHEMICAL BIOLOGY
CANCER
COLLECTIVE CELL MIGRATION
MESENCHYMAL MIGRATION

Received
22 August 2012

Accepted
17 October 2012

Published
8 November 2012

Correspondence and requests for materials should be addressed to M.I. (imoto@bio.keio.ac.jp)

A chemical genomic study identifying diversity in cell migration signaling in cancer cells

Shigeyuki Magi, Etsu Tashiro & Masaya Imoto

Department of Biosciences and Informatics, Faculty of Science and Technology, Keio University, 3-14-1 Hiyoshi, Kohoku-ku, Yokohama 223-8522, Japan.

The aim of this study was to analyze the diversity and consistency of regulatory signaling in cancer cell migration, using a chemical genomic approach. The effects of 34 small molecular compounds were assessed quantitatively by wound healing assay in ten types of migrating cells. Hierarchical clustering was performed on the subsequent migration inhibition profile of the compounds and cancer cell types. The result was that hierarchical clustering accurately classified the compounds according to their targets. Furthermore, the cancer cells tested in this study were classified into three clusters, and the compounds were grouped into four clusters. An inhibitor of JNK suppressed all types of cell migration; however, inhibitors of ROCK, GSK-3 and p38MAPK only inhibited the migration of a subset of cell lines. Thus, our analytical system could easily distinguish between the common and cell type-specific signals responsible for cell migration.

Cell migration is central to many physiological processes, including development, tissue remodeling, and immune responses, and is also a required step in cancer metastasis. When a cell moves, multiple intracellular signaling networks control cell morphology. Signaling can be initiated through receptor tyrosine kinases, G protein-coupled receptors (GPCRs), integrin, and other receptors. These receptors are upregulated by extracellular stimuli that induce the activation of one or more intermediate signaling network branches. Finally, this signaling reaches the Rho family of small GTPase proteins. Many molecules and pathways have been implicated in intermediate signaling. For example, the Ras/Raf/MEK/ERK pathway has been reported to enhance cell motility[1–4]. In addition to the Ras/Raf/MEK/ERK pathway, a phosphoinositide 3-OH kinase (PI3K)/Akt pathway is widely known to regulate cell migration. This pathway is considered to be necessary for both Cdc42- and Rac1-induced cell motility and invasiveness[5], and it regulates the expression of Snail, which can increase cell motility[6]. Jun NH2-terminal kinase (JNK) and p38 mitogen-activated protein kinase (p38MAPK) have also been reported to play important roles in the signaling mechanisms involved in migration[7,8]. The role of Rho family small GTPase proteins, which is considered to constitute the final stage of the migration-signaling network, is known to regulate actin nucleation and polymerization. In particular, RhoA, Rac1, and Cdc42 are the major regulators of cytoskeletal remodeling. Activation of RhoA increases cell contractility and leads to the formation of focal adhesions and stress fibers[9]. Rac1 and Cdc42 activation induce the lamellipodia and filopodia, respectively[10,11]. Thus, the core elements of the intracellular migration-signaling network have been demonstrated.

However, it is likely that signaling molecules regulating cell migration in one cancer cell may not regulate cell migration in other genetically distinct cancer cells. Indeed, the PI3K/Akt pathway, but not the MEK/ERK pathway, has been shown to be critical for prostate cancer cell migration[6]. Other studies have reported that the constitutive activation of the MEK/ERK pathway by oncogenic mutations of $BRaf^{V600E}$ significantly induced cell migration through activation of RhoA GTPase[12]. In addition, the role of the Rho family of proteins in cell migration depends on specific cellular circumstances. The migration of several types of cancer cell is based on reorganization of the actin cytoskeleton, but their requirements for Rho and Rac signaling differ. With respect to a particular subset of cancer cells, cells migrated in a Rac-dependent manner, but Rho signaling was not essential. With respect to another subset of cancer cells, the inhibition of Rho/Rock signaling inhibited cell migration. Thus, although the same basic process of cell migration is induced, each type of cancer cell brings about migration in different contexts using distinct molecular repertoires. Therefore, understanding the diversity and commonality of signaling pathways that regulate cell migration in various cell types is important not only for basic research into cell migration, but also for the development of anti-metastatic anti-tumor drugs.

Table 1 | The experimental conditions of the wound healing assays for each cell line

Cell line	Origin	Cell number (cells/well)	Migration factor
A431	Human epithelial carcinoma	7.5×10^4	EGF 3 ng/ml or EC17-CM
EC17	Human esophageal carcinoma	7.5×10^4	None
EC109	Human esophageal carcinoma	7.5×10^4	EGF 3 ng/ml or EC17-CM
HT1080	Human fibrosarcoma	7.5×10^4	FBS (2%)
TE8	Human esophageal carcinoma	7.5×10^4	EGF 3 ng/ml
TT	Human medullary thyroid carcinoma	7.5×10^4	EGF 3 ng/ml
3Y1	Rat fibroblast	7.5×10^4	FBS (5%)
B16	Mouse melanoma	2.2×10^5	EC17-CM

To address this issue, we utilized the chemical genomic approach in which chemical inhibitors were used as probes to mimic loss-of-function phenotypes by inhibiting target protein activity; that is, if a chemical inhibitor suppresses the cell migration of one type of cancer cell, the target protein of the inhibitor can be considered as being involved in the mechanism of cell migration of that type of cell. This chemical genetic approach is easily applicable to different cell models; therefore, it can determine which signaling molecule is universally involved in the migration mechanism in several types of cancer cells, and which one is specifically involved in each type of cell. In the present study, we first examined the effects of various chemical inhibitors on cell migration in several cancer cell models, and subsequently obtained chemosensitive migratory profiles and undertook cluster analysis to classify the signaling molecules and their inhibitors as being either common to all cancer cells or specific to certain cell types.

Results

Determination of appropriate experimental conditions for the wound healing assay. To select the cell models used in this study, sixteen cell lines, including colon carcinoma, esophageal carcinoma and lung cancer, were assessed with regard to their migration ability in response to migration factors using a wound healing assay[13]. The assay conditions of each cell line were optimized by examining migration factors such as growth factors, cell number required to maintain a confluent cell monolayer, and an assay duration that clearly revealed the extent of motility. We found out that the eight cell lines were suitable for use in a migration assay under the conditions indicated in **Table 1** (see also the Methods section). We also confirmed that both number of alive and dead cells in each condition were not clearly increased in optimized assay condition. The other cell lines tested were not affected by migratory stimuli or could not be scratched. Among the eight cell lines selected, EC17 cells migrated without extracellular stimulation, indicating that EC17 cells secrete chemoattractants into the media, and acquire motility by autocrine signaling. Conversely, others required the addition of migration factors, such as epidermal growth factor (EGF), conditioned medium from EC17 cells (EC17-CM), or serum (**Figure 1a**). A431 cells and EC109 cells migrated in response to both EGF and EC17-CM. **Figure 1b** shows the morphology of migration in these cell lines. A431 cells and EC109 cells moved together in sheet-like structures (collective migration), whereas the other cell lines showed a fibroblast-like spindle-shaped morphology and migrated individually like mesenchymal cells (mesenchymal migration).

Signaling pathway regulating for cell migration differs among three cancer cell lines. Next, to examine whether our analytical system could distinguish between common signals responsible for cell migration in the cancer cells tested and cell type-specific signals, using signal transduction inhibitors, a test was done using A431 cells, EC109 cells or TT cells that were randomly selected to analyze their migration ability. This was conducted following treatment with three

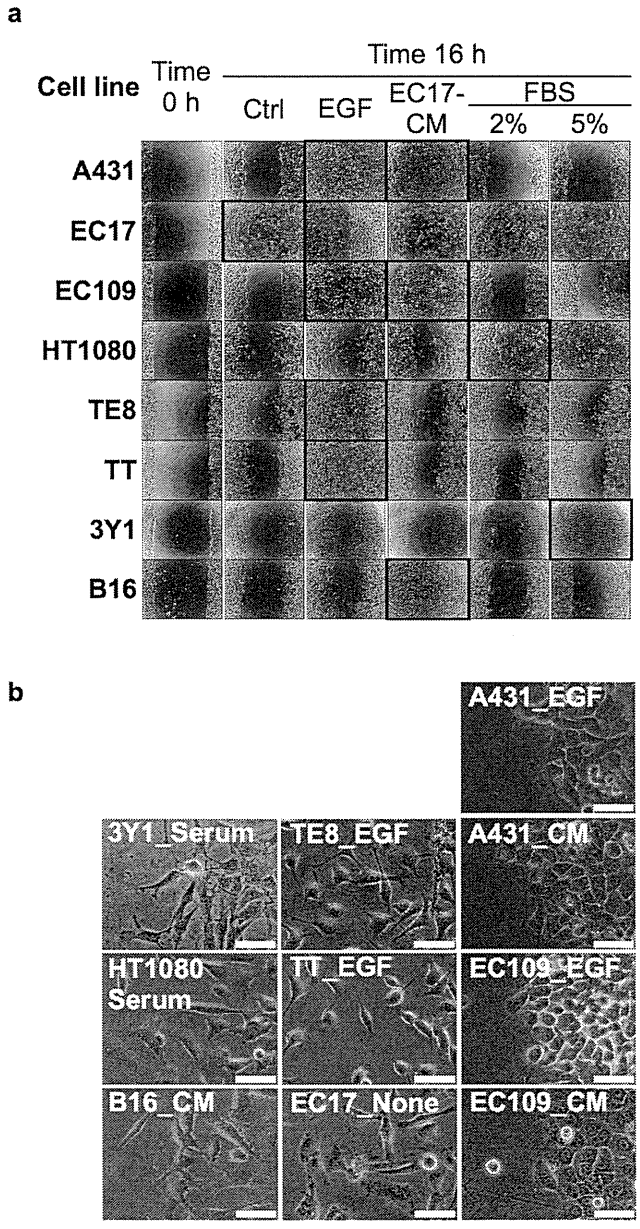

Figure 1 | The effect of migratory stimuli on cell migration in various cell lines. (a) Cells were scratched and then stimulated by EGF (3 ng/mL), serum, or conditioned medium from EC17 cells. After 16 h, wound areas were observed and photographed under microscopy. (b) Images of cell lines treated with migratory stimuli. Cells were photographed 10 h after stimulation. The scale bar represents 50 μm.

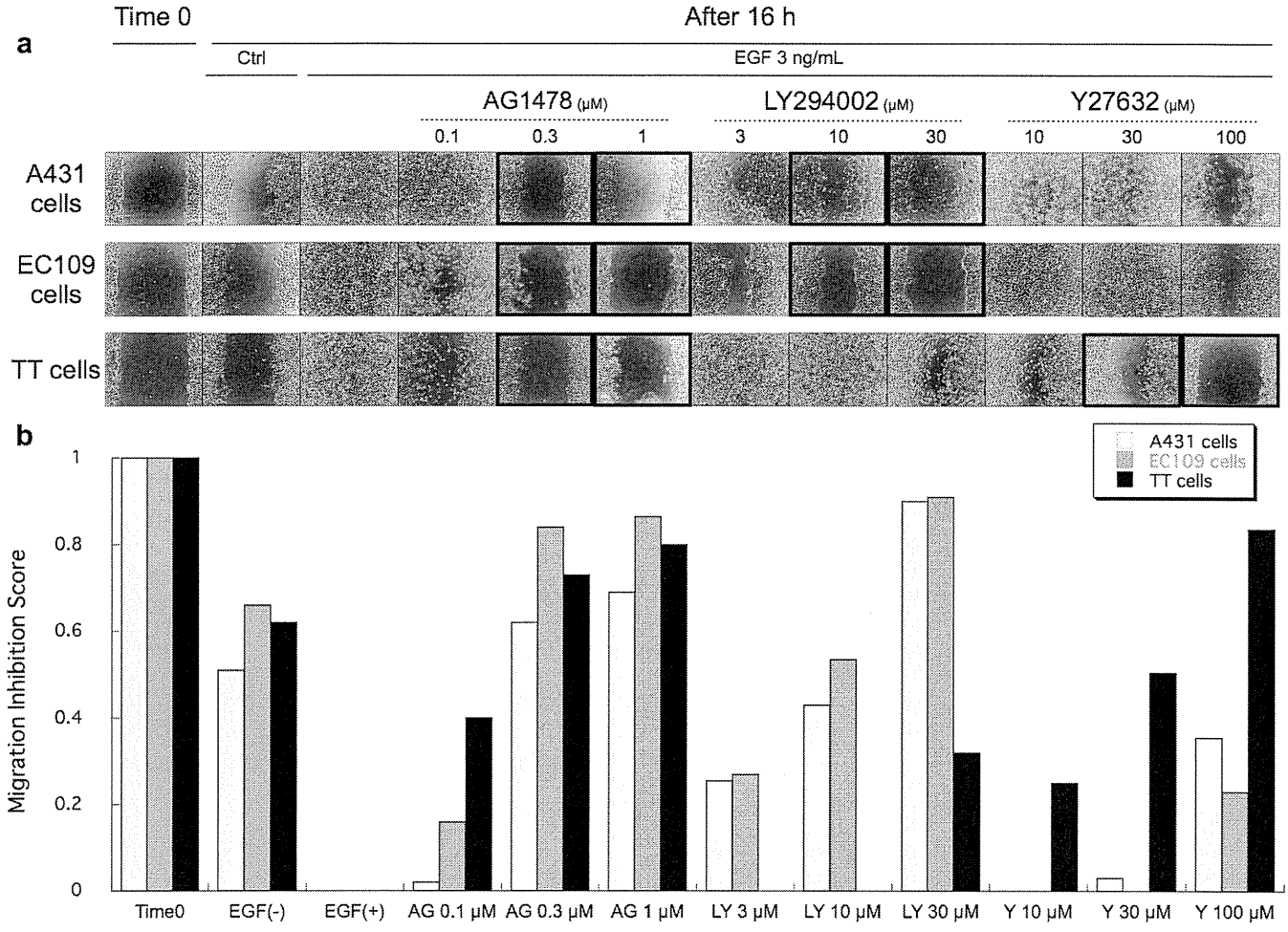

Figure 2 | The inhibitory pattern of cell migration was dependent on the types of cancer cell line. A confluent monolayer of A431 cells, EC109 cells, and TT cells were scratched, treated with AG1478, LY294002, or Y27632, and stimulated with EGF as described in the Methods section. (a) Wound areas were photographed just after scratching (time zero). After 16 h, wound areas were photographed again (others). Black boxes indicate the inhibitory effects of chemicals on cell migration. The data were representative of two independent studies. (b) Migration inhibition score (MIS) of each experimental condition. MIS was quantified by measurement of the cell-free area in the picture. The quantified value was normalized against the value at time zero. The data were the average of two independent studies.

kinase inhibitors; PI3K inhibitor, Rho-associated kinase (ROCK) inhibitor and EGF receptor kinase inhibitor. The reason why we focused on the inhibitors of PI3K and ROCK for this test was that PI3K and ROCK were expected to reveal cell type-specific effects on migration. This is because they have been reported to be involved in regulation mechanisms of cell migration that are initiated downstream to growth factor signaling in a subset of cancer cells[5,14], although they were also reported to be dispensable for migration or membrane ruffling in certain conditions[15,16]. **Figure 2a** presents the effect of these three inhibitors on the EGF-induced motility of A431 cells, EC109 cells, and TT cells. The extent of the cell motility was quantified by the measurement of the cell-free area in a photograph. The quantified value was calculated over a fixed period of time, and was termed the 'migration inhibition score (MIS)' (**Figure 2b**). These results indicated that the EGF receptor kinase inhibitor, AG1478, inhibited the EGF-induced migration of all three cell lines, as expected. The PI3K inhibitor and LY294002 suppressed the EGF-induced migration of A431 cells and EC109 cells, but not of TT cells, indicating that PI3K plays a critical role in EGF-induced cell migration in A431 cells and EC109 cells. In contrast, the ROCK inhibitor, Y27632, suppressed migration only in A431 cells and TT cells, indicating that ROCK is indispensable for EGF-induced cell migration in A431 cells and TT cells but not in EC109 cells. Thus, our analytical system using chemical inhibitors of signal transduction easily distinguished between common and cell type-specific signals responsible for cell migration.

Two-way cluster analysis of migration inhibition score. To reveal the diversity and generality of regulatory signaling in cancer cell migration, we tested the effect of 34 different signal transduction inhibitors on the migration of ten types of cells, as shown in Table 1. Table 2 lists the names of the chemical inhibitors of signal transduction used in this study, the experimental concentrations of each inhibitor, and their modes of action. Each inhibitor was used at three concentrations, the highest one being a concentration just below the level that would affect cell viability. Using these chemical inhibitors under the stated concentrations, we carried out two highly reproducible, independent experiments on each cell line ($r = 0.94$, p-value $< 2.2 \times 10^{-16}$, **Figure 3**), and provided a final dataset by averaging the data points from the two experiments. The MIS dataset is shown in Supplementary Table 1. Then a hierarchical cluster analysis was performed. The results are displayed in the form of a heat map and a tree diagram (**Figure 4**). The heat map employs a gradient color scale from green, indicating MIS = 0, to magenta, indicating MIS = 1.0, interpolated over black indicating MIS = 0.5.

As a result of these experiments, the characteristic features of cell migration affected by chemical inhibitors in cancer cells were

Table 2 | Compound concentrations and targets of inhibition used in this study

Compound name	Concentration	Target / Mode of action	References
A23187	30, 100, 300 nM	Ca^{2+} Ionophore	33
AA861	3, 10, 30 μM	5-Lipoxygenase	34
AG1478	0.1, 0.3, 1 μM	EGFR	35
Alendronate	10, 30, 100 μM	FPP synthase	36
ALLN	1, 3, 10 μM	Calpain	37
Bafilomycin A	0.3, 1, 3 nM	V-ATPase	38
Cytochalasin D	0.1, 0.3, 1 μM	Actin polymarization	39
Herbimycin A	1, 3, 10 μg/mL	Hsp90	40
Leptomycin B	0.1, 0.3, 1 ng/mL	CRM1	41
LY294002	3, 10, 30 μM	PI3K	42
Mevastatin	3, 10, 30 μM	HMG-CoA reductase	43
Moverastin	3, 10, 30 μM	Farnesyl transferase	20
MG132	10, 30, 100 nM	Proteasome	44
MK571	3, 10, 30 μM	CysLT1	45
MK886	1, 3, 10 μM	FLAP	46
Okadaic acid	3, 10, 30 nM	PP2A	47
Paclitaxel	30, 100, 300 ng/mL	Tubulin depolymerization	48
PD169316	1, 3, 10 μM	p38MAPK	49
Radicicol	1, 3, 10 μg/mL	Hsp90	50
Rapamycin	1, 3, 10 μg/mL	mTOR	51
Risedronate	30, 100, 300 μM	FPP synthase	36
SB203580	3, 10, 30 μM	p38MAPK	52
SB218078	30, 100, 300 nM	Chk1	53
SB415286	3, 10, 30 μM	GSK-3	54
SP600125	1, 3, 10 μM	JNK	55
Thapsigargin	3, 10, 30 nM	Ca^{2+}-ATPase	56
Trichostatin A	30, 100, 300 ng/mL	Histone deacetylase	57
Tunicamycin	30, 100, 300 ng/mL	Glycosylation	58
U0126	3, 10, 30 μM	MEK	59
UTKO1	1, 3, 10 μM	14-3-3	22
Vinblastine	3, 10, 30 ng/mL	Tubulin polymerization	60
Wortmannin	0.3, 1, 3 μM	PI3K	61
Xanthohumol	0.3, 1, 3 μg/mL	Valosin-containing protein	23
Y27632	10, 30, 100 μM	ROCK	62

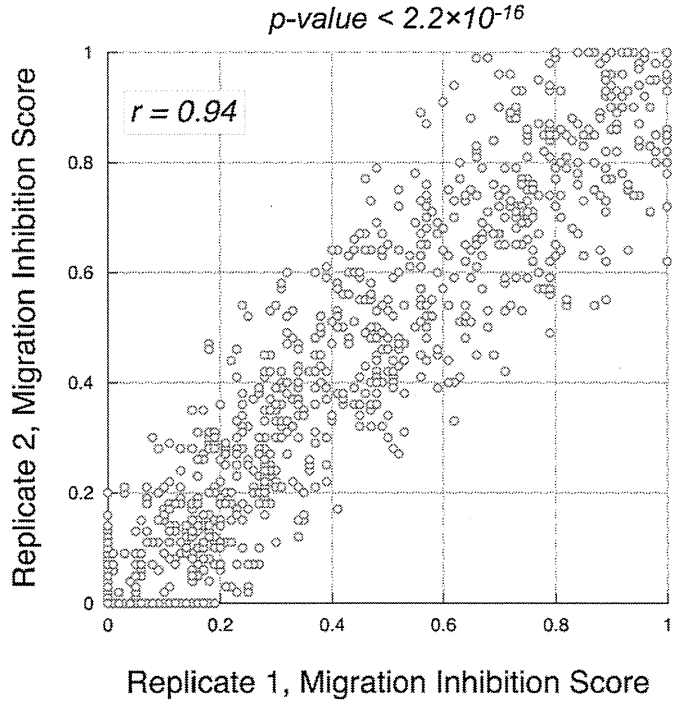

Figure 3 | Reproducibility of the migration inhibition score. Before averaging, two independent data sets were checked for high correlation ($r = 0.94$, p-value $< 2.2 \times 10^{-16}$).

classified into three general clusters (**Figure 4a**). Cluster A consisted of three types of cells and cell migration properties: B16 cells, HT1080 cells, and 3Y1 cells; their cell migration displayed lower sensitivities to the inhibitors tested in this study than the others (**Figure 4b**). Cluster B consisted of cell migration of A431 cells and EC109 cells stimulated with either EGF or EC17-CM. The EGF-induced chemosensitive migratory profile of these cells was similar to that induced by EC17-CM. Cluster C consisted of three types of cells: EC17 cells, TE8 cells and TT cells.

It was expected that the chemical inhibitors that targeted the same molecule would be clustered into the same tree. Indeed, PD169316 and SB203580 as p38MAPK inhibitors, herbimycin A and radicicol (Hsp90 inhibitors), LY294002 and wortmannin (PI3K inhibitors), paclitaxel and vinblastine (tubulin binders), and alendronate and risedronate (farnesyl diphosphate (FPP) synthase inhibitors), were all clustered into the same position (indicated by gray boxes). These results indicate that our chemical genomic approach was able to classify the chemical inhibitors based on their respective modes of action, similar to previous studies on the chemosensitivities of cancer cells[17–19].

Furthermore, the chemical inhibitors used in this study were classified into four general clusters (**Figure 4b**), and each inhibitor in **Figure 4b** can be linked to its target molecule. We also displayed the relationships of the targets of the inhibitors as a non-root phylogenetic tree (**Figure 4c**). The inhibitors grouped into cluster 1 contained the 5-lipoxygenase-activating protein (FLAP) inhibitor, MK886, the vacuolar-type proton-ATPase (V-ATPase) inhibitor, bafilomycin A, and the FPP synthase inhibitors, the bisphosphonates. These inhibitors showed little inhibitory effect on cell migration in almost all cell types, thus the target molecules of these compounds had little bearing

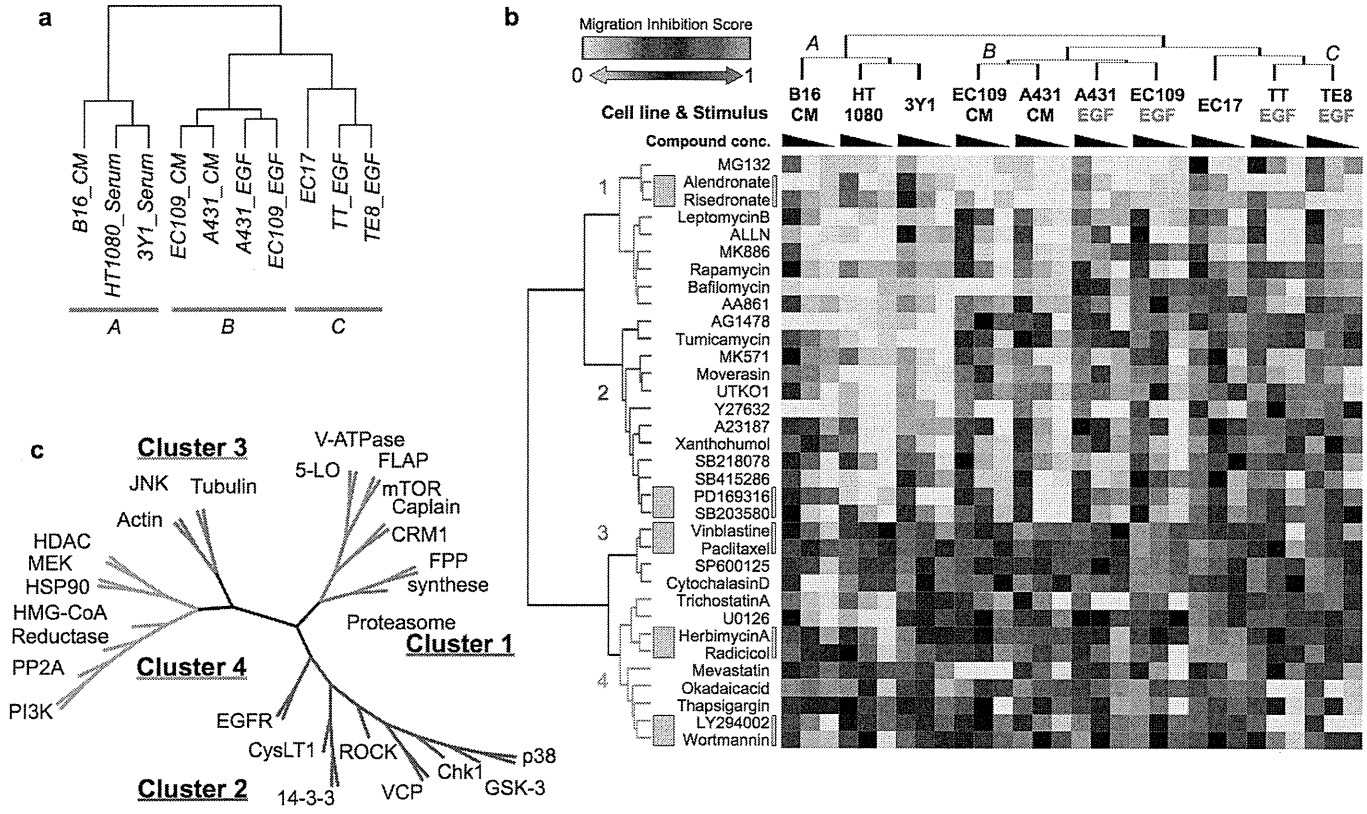

Figure 4 | Cluster analysis of the chemosensitivity profile of migration inhibition. Cluster analysis was performed using Euclidean distance and Ward's method. (a) The MIS dataset was clustered into ten types of cell migration. Cell migration types were classified into three general clusters; clusters A, B, and C. (b) The MIS dataset was hierarchically clustered using data from 34 compounds. Rows indicate 34 different small molecular compounds. Columns indicate the ten migration types, including the three different compound concentrations. The heat map shows a gradient color scale from green, indicating MIS = 0, to magenta, indicating MIS = 1, interpolated over black for MIS = 0.5. Gray boxes beside the heat map indicate that two labeled compounds have almost the same molecular target. The 34 compounds were clustered into four general groups. (c) The non-rooted phylogenetic tree classifies the target molecules of the small molecular compounds tested in this study. Each small compound inhibitor used in this study can be replaced with its target molecule because most targets have already been identified. This phylogenetic tree presents the distances between molecules on the signaling network contributing to cell migration.

on the regulating mechanisms of cell migration tested in this study. Cluster 2 contained Y27632, AG1478, the p38MAPK inhibitors, the chk1 inhibitor, SB218078 and so on. Most of these compounds showed a stronger inhibitory effect on cell migration, classified into migration type clusters B and C, in contrast to cluster A. Therefore, the target molecules of these compounds were not involved in the migration of HT1080 cells and 3Y1 cells but they did regulate cell migration in the subset of cell lines grouped into clusters B and C. Cluster 3 contained SP600125 and the cytoskeleton-affecting compounds. This group of inhibitors affected all types of cell migration, indicating that not only cytoskeletal molecules, but also JNK, are common regulators of cell migration, irrespective of cell type. Cluster 4 contains the Hsp90 inhibitors, the MEK inhibitor, U0126, and the PI3K inhibitors. These inhibitors also suppressed migration in all types of cell with different potencies depending on cell type. Thus the target molecules of these inhibitors also played a common role in all types of cell migration.

Discussion

In the present study, we investigated some general and specific regulatory mechanisms of cell migration. To accomplish our objective, we assessed the effects of 34 different kinds of chemical inhibitors on the migration of ten types of cells using a wound healing assay, and subsequently performed a cluster analysis on the dataset. One significant aspect of this work is that each compound showed a characteristic cell type-specific inhibitory pattern on migration, and hierarchical clustering precisely classified the compounds according to their respective targets, such as p38, Hsp90, PI3K, tubulin and FPP synthase (**Figure 4b, c**). Therefore, our research could be applied to predict the mode of action of each compound. For example, moverastin and its derivative UTKO1 were classified into same cluster, in spite of the different functions of these two compounds, which have similar structures. We previously reported that moverastin was an inhibitor of farnesyltransferase[20], and it inhibited cell migration by inhibiting farnesylation in H-Ras. On the other hand, UTKO1 was reported not to inhibit farnesyltransferase[21], but it directly bound to 14-3-3ζ, and inhibited the interaction between the 14-3-3 proteins and Tiam1, a protein that has been reported to be a Rac-specific GEF. This resulted in the inhibition of Rac1[22]. Therefore, it has been demonstrated that the migration of epithelial cells requires Taim1-mediated Rac1 activation. However, because our profiling data demonstrated that moverastin and UTKO1 were classified in the same cluster, we examined the possibility that moverastin could bind to 14-3-3ζ, and obtained similar results (data not shown). Therefore it is likely that moverastin might inhibit cell migration not only by inhibiting protein farnesylation, but also by inhibiting Tiam1-mediated Rac1 activation. In addition, because the CysLT1 antagonist MK571 was classified into the same cluster as moverastin and UTKO1, this raised the possibility that CysLT1 signaling might be closely related to Taim1-mediated Rac1 activation. We therefore examined this potential mode of action, and found that EGF-induced Rac1 activation was regulated by CysLT1 signaling (unpublished

data). Thus, our profiling data appeared to be helpful in the mechanistic study of cell migration. At the same time, our clustering data indicated that xanthohumol was grouped in the same category as the Ca^{2+} ionophore, A23187. Recently, xanthohumol was reported to bind to and inhibit valosin-containing protein (VCP)[23], resulting in the induction of ER stress. Although A23187 is also a well-known inducer of ER stress[24,25], other ER stress-inducing compounds such as tunicamycin and thapsigargin were classified into different clusters from xanthohumol and A23817. Therefore, an interpretation of the clustering data must be made with great caution.

The characteristics of cell migration based on chemical inhibitor-sensitivity profiles were grouped into three clusters (clusters A, B and C), and chemical inhibitors were classified into four general groups (clusters 1 to 4, **Figure 4**). Although the motilities of several cell lines we tested are upregulated by extracellular stimuli such as EGF, they migrated a little without stimulation (**Figure 1a**). Additionally, EC17 cells did not require extracellular stimulation to migrate. Thus we just have to evaluate and discuss chemical inhibitor-sensitivity profiles as total effects on "basal" and "stimulated" motility. JNK inhibitor, tubulin and actin polymerization inhibitors in cluster 3 showed a potent inhibitory effect on migration of all cell types, indicating that JNK is a common and crucial signaling molecule regulating cell migration. Indeed, JNK was reported to modulate migration in a broad range of cell types[26], such as keratinocytes[7], neuronal cells[27], and many cancer cell lines[28,29]. Because dynamic reorganization of the actin cytoskeleton is considered to be key to the cell's capacity to migrate[30], JNK may be indispensable for the phosphorylation of paxillin and F-actin polymerization[7,8].

In contrast, some of the chemical inhibitors classified into cluster 2 (AG1478, tunicamycin, the CysLT1 antagonist MK571, Moverastin and UTKO1) affected the migration of cell lines of epithelial origin (EC109 cells, A431 cells, EC17 cells, TT cells, TE8 cells) in clusters B and C, but did not affect the migration of cell lines of mesenchymal origin (HT1080 cells and 3Y1 cells) placed in cluster A. This suggests that there is an essentially different regulatory mechanism of cell migration between cells of these two origins. The regulatory mechanism of cell migration of B16 cells appeared somewhat similar to that of cell lines of mesenchymal origin when compared to those with an epithelial origin.

Moreover, although EGF did induce migration of cells of epithelial origin (TT cells, TE8 cells, A431 and EC109 cells), differential sensitivities to several inhibitors was observed in A431 and EC109 cells in cluster B and TT cells and TE8 cells in cluster C. These results suggest that the EGF signaling pathway leading to migration of A431 and EC109 cells in cluster B was not identical to that of TT cells and TE8 cells in cluster C. Furthermore, EC17-CM also induced migration of A431 and EC109 cells with a similar chemosensitive profile to that seen in EGF-induced migration, indicating that EC17-CM might activate almost the same signaling pathway as the EGF-signaling pathway in the context of the migration of these cells. One exception is AA861, an inhibitor of 5-lipoxygenase (5-LO). AA861 inhibited the EGF-induced migration of A431 cells and EC109 cells, but not EC17-CM-induced migration. Therefore, production of leukotriene(s) catalyzed by 5-lipoxygenase is required for EGF-induced cell migration, whereas EC17-CM may already contain leukotriene(s), so EC17-CM-induced cell migration was not inhibited by inhibition of 5-LO. In addition, a specific inhibitor of EGF-receptor tyrosine kinase (AG1478) potently inhibited the EC17-CM-induced migration of A431 and EC109 cells, but weakly inhibited migration of EC17 cells, indicating that EC17 cells might produce and secrete EGF, whereas EC17 cells underwent cell migration in response to migration factors other than EGF.

Interestingly, the mode of EGF-induced cell migration based on cell morphology can also be classified into clusters B and C. As shown in **Figure 1b**, A431 cells and EC109 cells in cluster B showed collective migration, whereas TT, TE8 and EC17 cells in cluster C showed a mesenchymal migration. With respect to collective migration, cells moved in groups and a leading cell at the tip of the group generated the migratory traction and the cells in the middle and at the back of the group were predominantly dragged passively. In contrast, mesenchymal migration required the formation of protrusions at the leading edge and actomyosin-mediated retraction of the trailing edge. This raises the possibility that the difference in the mode of cell migration of epithelial cells might be correlated with the differences in sensitivity to chemical inhibitors between clusters B and C. The ROCK inhibitor, Y27632, is a representative example; it inhibited mesenchymal migration of TT cells and TE8 cells more potently than collective migration of A431 and EC109 cells. Indeed, Rho-ROCK signaling is proposed to induce actomyosin-mediated retraction at the trailing edge in mesenchymal migration[15]. As an exception, the ROCK inhibitor Y27632 failed to inhibit mesenchymal migration of EC17 cells. At present, although we do not know why inhibition of ROCK did not suppress the migration of EC17 cells, one possible explanation is that another Rho effector, citron kinase or mDia, could regulate mesenchymal migration if used instead of ROCK. Moreover, the GSK-3 inhibitor (SB415286) and the p38MAPK inhibitors (PD169316 and SB203580) also inhibited the EGF-induced migration of TE8, TT, and EC17 cells more potently than they did in A431 and EC109 cells. This indicates that GSK3 and p38MAPK might be involved in the Rho-ROCK signaling responsible for mesenchymal migration. These ideas can be supported by other findings. GSK-3 phosphorylated and inactivated p190A RhoGAP, which is a key Rho regulatory protein in the context of cell migration. This resulted in the activation of Rho-ROCK signaling[31]. Furthermore, the phosphorylation of protein substrates by GSK-3 often requires the "priming" of a neighboring residue by a distinct kinase, leading to subsequent phosphorylation by GSK-3[32]. p38MAPK could effectively prime the C-terminal fragment of p190A RhoGAP for subsequent phosphorylation by GSK-3. The Chk1 inhibitor SB218078 also inhibited EGF-induced migration of TE8, TT, and EC17 cells more potently than it did in A431 and EC109 cells. However, at present we do not know how chk1 is involved in mesenchymal migration. Moreover, we cannot exclude the possibility that chk1 is important in mechanisms other than the mode of cell migration. Contrastingly, although PI3K, PP2A and HMG-CoA reductase somewhat selectively inhibited EGF-induced collective migration, the role of these enzymes on cell migration remains unclear.

In summary, we have shown that JNK is a signaling molecule common to all types of cell migration, and many molecules have diverse functions in the migration of particular types of cancer cells. We determined this using a chemical genomic approach. Our approach can be used as a tool for understanding the diversity and similarities in cancer cell migration signaling, opening up the potential for revealing novel molecular targets in cancer therapy.

Methods

Cell culture. 3Y1 and HT1080 cells were maintained in Dulbecco's Eagle's medium (DMEM) supplemented with 10% fetal bovine serum (FBS), 0.1 g/l kanamycin, 100 units/ml penicillin G, 0.6 g/l L-glutamine, and 2.5 g/l $NaHCO_3$. A431 cells were maintained in DMEM supplemented with 5% calf serum (CS), 0.1 g/l kanamycin, 100 units/ml penicillin G, 0.6 g/l L-glutamine, and 2.5 g/l $NaHCO_3$. B16 cells were maintained in DMEM supplemented with 8% FBS, 0.1 g/l kanamycin, 100 units/ml penicillin G, 0.6 g/l L-glutamine, and 2.5 g/l $NaHCO_3$. EC17, EC109, TE8, and TT cells were maintained in Roswell Park Memorial Institute (RPMI) medium 1640 supplemented with 5% FBS, 0.1 g/l kanamycin, 100 units/ml penicillin G, 0.6 g/l L-glutamine, and 2.5 g/l $NaHCO_3$. For routine culture, cells were incubated in a standard humidified incubator at 37°C in 5% CO_2.

Reagents. A23187, AG1478, ALLN, cytochalasin D, okadaic acid, rapamycin, and Y27632 were purchased from Calbiochem. MK571 was purchased from Cayman. Thapsigargin was purchased from Santa Cruz Biotechnology. AA861, bafilomycin A, LY294002, mevastatin, MG132, MK886, PD169316, SB203580, SB218078, SB415286, SP600125, tunicamycin, U0126, wortmannin, and epidermal growth factor were purchased from Sigma. Paclitaxel, radicicol, and vinblastine were purchased from Wako Pure Chemical Industries, Ltd. Herbimycin A, moverastin, and xanthohumol was purified from cultures of *Streptomyces sp.* in our own laboratory. Leptomycin B

and trichostatin A were kind gifts from Dr. Minoru Yoshida at RIKEN. Compound UTKO1 was synthesized and kindly donated by Dr. Hidenori Watanabe of the University of Tokyo. Alendronate and risedronate were kind gifts from Yamanouchi Pharmaceutical Co., Ltd (Astellas Pharma Inc.).

Preparation of conditioned medium (CM) from EC17 cells. EC17 cells (1.0×10^6 cells) were seeded in ϕ 100 mm dish. The following day, the medium was replaced with 10 ml of RPMI 1640 containing 1% FBS. After 24 h, the medium was recovered and sterilized by filtration.

Wound healing assay. A confluent monolayer of cells in a 48-well plate was scratched with a micropipette tip to create a cell-free zone in each well, about 1 mm in width. The medium was replaced with RPMI1640 with 1% FBS with or without test compound, and cells were either treated with the migratory stimulus or not treated with it so as to serve as controls. After a fixed period of time, cells were observed and photographed under a microscope. The experimental conditions for each cell line are described as Table 1. Wound areas were quantified using ImageJ software. After photographing, cells were trypsinized and collected, and cell viability was determined by trypan blue dye exclusion assay. Average migration inhibition scores were calculated from two independent experiments.

Cluster analysis. The value of migration inhibition was ordered according to the experimental conditions of cell migration or the compounds used. These profiles were analyzed by hierarchical clustering (using the method of Ward's linkage based on Euclidean distance) and visualized using a heat map using the R Project package (http://www.R-project.org).

1. Marshall, C. J. Ras effectors. *Curr. Opin. Cell Biol.* **8**, 197–204 (1996).
2. Klemke, R. L. *et al.* Regulation of cell motility by mitogen-activated protein kinase. *J. Cell Biol.* **137**, 481–492 (1997).
3. Nguyen, D. H. *et al.* Myosin light chain kinase functions downstream of Ras/ERK to promote migration of urokinase-type plasminogen activator-stimulated cells in an integrin-selective manner. *J. Cell Biol.* **146**, 149–164 (1999).
4. Tanimura, S. *et al.* Prolonged nuclear retention of activated extracellular signal-regulated kinase 1/2 is required for hepatocyte growth factor-induced cell motility. *J. Biol. Chem.* **277**, 28256–28264 (2002).
5. Keely, P. J., Westwick, J. K., Whitehead, I. P., Der, C. J. & Parise, L. V. Cdc42 and Rac1 induce integrin-mediated cell motility and invasiveness through PI(3)K. *Nature* **390**, 632–636 (1997).
6. Gan, Y. *et al.* Differential roles of ERK and Akt pathways in regulation of EGFR-mediated signaling and motility in prostate cancer cells. *Oncogene* **29**, 4947–4958 (2010).
7. Huang, C., Rajfur, Z., Borchers, C., Schaller, M. D. & Jacobson, K. JNK phosphorylates paxillin and regulates cell migration. *Nature* **424**, 219–223 (2003).
8. Wagner, E. F. & Nebreda, A. R. Signal integration by JNK and p38 MAPK pathways in cancer development. *Nat. Rev. Cancer* **9**, 537–549 (2009).
9. Narumiya, S., Ishizaki, T. & Watanabe, N. Rho effectors and reorganization of actin cytoskeleton. *FEBS Lett.* **410**, 68–72 (1997).
10. Nobes, C. D. & Hall, A. Rho, rac, and cdc42 GTPases regulate the assembly of multimolecular focal complexes associated with actin stress fibers, lamellipodia, and filopodia. *Cell* **81**, 53–62 (1995).
11. Etienne-Manneville, S. & Hall, A. Rho GTPases in cell biology. *Nature* **420**, 629–635 (2002).
12. Makrodouli, E. *et al.* BRAF and RAS oncogenes regulate Rho GTPase pathways to mediate migration and invasion properties in human colon cancer cells: a comparative study. *Mol. Cancer* **10**, 118 (2011).
13. Yarrow, J. C., Totsukawa, G., Charras, G. T. & Mitchison, T. J. Screening for cell migration inhibitors via automated microscopy reveals a Rho-kinase inhibitor. *Chem. Biol.* **12**, 385–395 (2005).
14. Kakinuma, N., Roy, B. C., Zhu, Y., Wang, Y. & Kiyama, R. Kank regulates Rho A-dependent formation of actin stress fibers and cell migration via 14-3-3 in PI3K-Akt signaling. *J. Cell Biol.* **181**, 537–549 (2008).
15. Sanz-Moreno, V. *et al.* Rac activation and inactivation control plasticity of tumor cell movement. *Cell* **135**, 510–523 (2008).
16. Kurokawa, K. *et al.* Coactivation of Rac1 and Cdc42 at lamellipodia and membrane ruffles induced by epidermal growth factor. *Mol. Biol. Cell* **15**, 1003–1010 (2004).
17. Scherf, U. *et al.* A gene expression database for the molecular pharmacology of cancer. *Nat. Genet.* **24**, 236–244 (2000).
18. Nakatsu, N. *et al.* Chemosensitivity profile of cancer cell lines and identification of genes determining chemosensitivity by an integrated bioinformatical approach using cDNA arrays. *Mol. Cancer Ther.* **4**, 399–412 (2005).
19. Muroi, M. *et al.* Application of proteomic profiling based on 2D-DIGE for classification of compounds according to the mechanism of action. *Chem. Biol.* **17**, 460–470 (2010).
20. Takemoto, Y. *et al.* Chemistry and biology of moverastins, inhibitors of cancer cell migration, produced by *Aspergillus*. *Chem. Biol.* **12**, 1337–1347 (2005).
21. Sawada, M. *et al.* Synthesis and anti-migrative evaluation of moverastin derivatives. *Bioorg. Med. Chem. Lett.* **21**, 1385–1389 (2011).
22. Kobayashi, H. *et al.* Involvement of 14-3-3 proteins in the second epidermal growth factor-induced wave of Rac1 activation in the process of cell migration. *J. Biol. Chem.* **286**, 39259–39268 (2011).
23. Sasazawa, Y. *et al.* Xanthohumol impairs autophagosome maturation through direct inhibition of valosin-containing protein. *ACS Chem. Biol.* (2012). doi:10.1021/cb200492h
24. Werno, C., Zhou, J. & Brüne, B. A23187, ionomycin and thapsigargin upregulate mRNA of HIF-1alpha via endoplasmic reticulum stress rather than a rise in intracellular calcium. *J. Cell Physiol.* **215**, 708–714 (2008).
25. Yamazaki, M., Chiba, K. & Yoshikawa, C. Genipin suppresses A23187-induced cytotoxicity in neuro2a cells. *Biol. Pharm. Bull.* **32**, 1043–1046 (2009).
26. Huang, C., Jacobson, K. & Schaller, M. D. A role for JNK-paxillin signaling in cell migration. *Cell Cycle* **3**, 4–6 (2004).
27. Sun, Y., Yang, T. & Xu, Z. The JNK pathway and neuronal migration. *J. Genet. Genomics* **34**, 957–965 (2007).
28. Ching, Y. P. *et al.* P21-activated protein kinase is overexpressed in hepatocellular carcinoma and enhances cancer metastasis involving c-Jun NH2-terminal kinase activation and paxillin phosphorylation. *Cancer Res.* **67**, 3601–3608 (2007).
29. Wang, J. *et al.* Sustained c-Jun-NH2-kinase activity promotes epithelial-mesenchymal transition, invasion, and survival of breast cancer cells by regulating extracellular signal-regulated kinase activation. *Mol. Cancer Res.* **8**, 266–277 (2010).
30. Pollard, T. D. & Borisy, G. G. Cellular motility driven by assembly and disassembly of actin filaments. *Cell* **112**, 453–465 (2003).
31. Jiang, W. *et al.* p190A RhoGAP is a glycogen synthase kinase-3-beta substrate required for polarized cell migration. *J. Biol. Chem.* **283**, 20978–20988 (2008).
32. Harwood, A. J. Signal transduction in development: holding the key. *Dev. Cell.* **2**, 384–385 (2002).
33. Abbott, B. J. *et al.* Microbial transformation of A23187, a divalent cation ionophore antibiotic. *Antimicrob. Agents Chemother.* **16**, 808–812 (1979).
34. Yoshimoto, T. *et al.* 2,3,5-Trimethyl-6-(12-hydroxy-5,10-dodecadiynyl)-1,4-benzoquinone (AA861), a selective inhibitor of the 5-lipoxygenase reaction and the biosynthesis of slow-reacting substance of anaphylaxis. *Biochim. Biophys. Acta.* **713**, 470–473 (1982).
35. Osherov, N. & Levitzki, A. Epidermal-growth-factor-dependent activation of the src-family kinases. *Eur. J. Biochem.* **225**, 1047–1053 (1994).
36. van Beek, E., Pieterman, E., Cohen, L., Löwik, C. & Papapoulos, S. Farnesyl pyrophosphate synthase is the molecular target of nitrogen-containing bisphosphonates. *Biochem. Biophys. Res. Commun.* **264**, 108–111 (1999).
37. Inoue, S., Bar-Nun, S., Roitelman, J. & Simoni, R. D. Inhibition of degradation of 3-hydroxy-3-methylglutaryl-coenzyme A reductase in vivo by cysteine protease inhibitors. *J. Biol. Chem.* **266**, 13311–13317 (1991).
38. Bowman, E. J., Siebers, A. & Altendorf, K. Bafilomycins: a class of inhibitors of membrane ATPases from microorganisms, animal cells, and plant cells. *Proc. Natl. Acad. Sci. USA* **85**, 7972–7976 (1988).
39. Cooper, J. A. Effects of cytochalasin and phalloidin on actin. *J. Cell Biol.* **105**, 1473–1478 (1987).
40. Whitesell, L., Mimnaugh, E. G., De Costa, B., Myers, C. E. & Neckers, L. M. Inhibition of heat shock protein HSP90-pp60v-src heteroprotein complex formation by benzoquinone ansamycins: essential role for stress proteins in oncogenic transformation. *Proc. Natl. Acad. Sci. USA* **91**, 8324–8328 (1994).
41. Nishi, K. *et al.* Leptomycin B targets a regulatory cascade of crm1, a fission yeast nuclear protein, involved in control of higher order chromosome structure and gene expression. *J. Biol. Chem.* **269**, 6320–6324 (1994).
42. Vlahos, C. J., Matter, W. F., Hui, K. Y. & Brown, R. F. A specific inhibitor of phosphatidylinositol 3-kinase, 2-(4-morpholinyl)-8-phenyl-4H-1-benzopyran-4-one (LY294002). *J. Biol. Chem.* **269**, 5241–5248 (1994).
43. Endo, A., Kuroda, M. & Tanzawa, K. Competitive inhibition of 3-hydroxy-3-methylglutaryl coenzyme A reductase by ML-236A and ML-236B fungal metabolites, having hypocholesterolemic activity. *FEBS Lett.* **72**, 323–326 (1976).
44. Lee, D. H. & Goldberg, A. L. Proteasome inhibitors: valuable new tools for cell biologists. *Trends Cell Biol.* **8**, 397–403 (1998).
45. Woszczek, G. *et al.* Functional characterization of human cysteinyl leukotriene 1 receptor gene structure. *J. Immunol.* **175**, 5152–5159 (2005).
46. Ford-Hutchinson, A. W. FLAP: a novel drug target for inhibiting the synthesis of leukotrienes. *Trends Pharmacol. Sci.* **12**, 68–70 (1991).
47. Bialojan, C. & Takai, A. Inhibitory effect of a marine-sponge toxin, okadaic acid, on protein phosphatases. Specificity and kinetics. *Biochem. J.* **256**, 283–290 (1988).
48. Schiff, P. B. & Horwitz, S. B. Taxol stabilizes microtubules in mouse fibroblast cells. *Proc. Natl. Acad. Sci. USA* **77**, 1561–1565 (1980).
49. Kummer, J. L., Rao, P. K. & Heidenreich, K. A. Apoptosis induced by withdrawal of trophic factors is mediated by p38 mitogen-activated protein kinase. *J. Biol. Chem.* **272**, 20490–20494 (1997).
50. Schulte, T. W. *et al.* Antibiotic radicicol binds to the N-terminal domain of Hsp90 and shares important biologic activities with geldanamycin. *Cell Stress Chaperones* **3**, 100–108 (1998).
51. Brown, E. J. *et al.* A mammalian protein targeted by G1-arresting rapamycin-receptor complex. *Nature* **369**, 756–758 (1994).
52. Gould, G. W., Cuenda, A., Thomson, F. J. & Cohen, P. The activation of distinct mitogen-activated protein kinase cascades is required for the stimulation of

2-deoxyglucose uptake by interleukin-1 and insulin-like growth factor-1 in KB cells. *Biochem. J.* **311** (Pt 3), 735–738 (1995).
53. Zhao, B. *et al.* Structural basis for Chk1 inhibition by UCN-01. *J. Biol. Chem.* **277**, 46609–46615 (2002).
54. Coghlan, M. P. *et al.* Selective small molecule inhibitors of glycogen synthase kinase-3 modulate glycogen metabolism and gene transcription. *Chem. Biol.* **7**, 793–803 (2000).
55. Han, Z. *et al.* c-Jun N-terminal kinase is required for metalloproteinase expression and joint destruction in inflammatory arthritis. *J. Clin. Invest.* **108**, 73–81 (2001).
56. Thastrup, O., Foder, B. & Scharff, O. The calcium mobilizing tumor promoting agent, thapsigargin elevates the platelet cytoplasmic free calcium concentration to a higher steady state level. A possible mechanism of action for the tumor promotion. *Biochem. Biophys. Res. Commun.* **142**, 654–660 (1987).
57. Yoshida, M., Kijima, M., Akita, M. & Beppu, T. Potent and specific inhibition of mammalian histone deacetylase both in vivo and in vitro by trichostatin A. *J. Biol. Chem.* **265**, 17174–17179 (1990).
58. Takatsuki, A., Arima, K. & Tamura, G. Tunicamycin, a new antibiotic. I. Isolation and characterization of tunicamycin. *J. Antibiot.* **24**, 215–223 (1971).
59. DeSilva, D. R. *et al.* Inhibition of mitogen-activated protein kinase kinase blocks T cell proliferation but does not induce or prevent anergy. *J. Immunol.* **160**, 4175–4181 (1998).
60. Owellen, R. J., Owens, A. H. & Donigian, D. W. The binding of vincristine, vinblastine and colchicine to tubulin. *Biochem. Biophys. Res. Commun.* **47**, 685–691 (1972).
61. Arcaro, A. & Wymann, M. P. Wortmannin is a potent phosphatidylinositol 3-kinase inhibitor: the role of phosphatidylinositol 3,4,5-trisphosphate in neutrophil responses. *Biochem. J.* **296** (Pt 2), 297–301 (1993).
62. Uehata, M. *et al.* Calcium sensitization of smooth muscle mediated by a Rho-associated protein kinase in hypertension. *Nature* **389**, 990–994 (1997).

Acknowledgements

We would like to thank Dr. M. Yoshida (RIKEN) for his kind gift of leptomycin B and trichostatin A; Dr. H. Watanabe (University of Tokyo) for his gracious gift of UTKO1; Dr. A. Funahashi (Keio University) for kind advice regarding data analysis. This work was supported by a Grant-in-Aid for Challenging Exploratory Research and JSPS Fellows, the Ministry of Education, Culture, Sports, Science, and Technology, Japan.

Author contributions

M.I. is responsible for project planning and experimental design; S.M. performed all of the experiments and statistical analyses; S.M., E.T. and M.I. co-wrote the paper.

Additional information

Competing financial interests: The authors declare no competing financial interests.

How to cite this article: Magi, S., Tashiro, E. & Imoto, M. A chemical genomic study identifying diversity in cell migration signaling in cancer cells. *Sci. Rep.* **2**, 823; DOI:10.1038/srep00823 (2012).

Citation: Blood Cancer Journal (2012) 2, e79; doi:10.1038/bcj.2012.26

www.nature.com/bcj

ORIGINAL ARTICLE

Identification of Toyocamycin, an agent cytotoxic for multiple myeloma cells, as a potent inhibitor of ER stress-induced XBP1 mRNA splicing

M Ri[1,5], E Tashiro[2,5], D Oikawa[3], S Shinjo[2], M Tokuda[3], Y Yokouchi[2], T Narita[1], A Masaki[1], A Ito[1], J Ding[1], S Kusumoto[1], T Ishida[1], H Komatsu[1], Y Shiotsu[4], R Ueda[1], T Iwawaki[3], M Imoto[2] and S Iida[1]

The IRE1α-XBP1 pathway, a key component of the endoplasmic reticulum (ER) stress response, is considered to be a critical regulator for survival of multiple myeloma (MM) cells. Therefore, the availability of small-molecule inhibitors targeting this pathway would offer a new chemotherapeutic strategy for MM. Here, we screened small-molecule inhibitors of ER stress-induced XBP1 activation, and identified toyocamycin from a culture broth of an *Actinomycete* strain. Toyocamycin was shown to suppress thapsigargin-, tunicamycin- and 2-deoxyglucose-induced XBP1 mRNA splicing in HeLa cells without affecting activating transcription factor 6 (ATF6) and PKR-like ER kinase (PERK) activation. Furthermore, although toyocamycin was unable to inhibit IRE1α phosphorylation, it prevented IRE1α-induced XBP1 mRNA cleavage *in vitro*. Thus, toyocamycin is an inhibitor of IRE1α-induced XBP1 mRNA cleavage. Toyocamycin inhibited not only ER stress-induced but also constitutive activation of XBP1 expression in MM lines as well as primary samples from patients. It showed synergistic effects with bortezomib, and induced apoptosis of MM cells including bortezomib-resistant cells at nanomolar levels in a dose-dependent manner. It also inhibited growth of xenografts in an *in vivo* model of human MM. Taken together, our results suggest toyocamycin as a lead compound for developing anti-MM therapy and XBP1 as an appropriate molecular target for anti-MM therapy.

Blood Cancer Journal (2012) **2,** e79; doi:10.1038/bcj.2012.26; published online 20 July 2012

Keywords: multiple myeloma; ER stress; IRE1α; XBP1; toyocamycin; adenosine analog

INTRODUCTION

Multiple myeloma (MM) is a hematological malignancy characterized by the accumulation of clonogenic mature plasma cells in bone marrow. Recently, bortezomib (BTZ), a proteasome inhibitor, was approved by the Food and Drug Administration for the treatment of MM. However, BTZ treatment often achieves only very short-duration responses and drug resistance tends to develop rapidly.[1,2] Therefore, there is a need to develop novel molecular targets for new therapeutic approaches.

Recent studies have suggested that XBP1, a basic region/leucine zipper (bZIP) transcription factor of the CREB-ATF family, has an important role in the survival of MM cells. XBP1 is required for the terminal differentiation of B lymphocytes to plasma cells and is essential for immunoglobulin secretion.[3,4] Abundant or deregulated expression of XBP1 has been detected in MM cells[5,6] and in hepatocellular carcinomas.[7,8] Because of the production of abundant immunoglobulins and cytokines, MM cells must be able to survive under conditions of chronic endoplasmic reticulum (ER) stress. This involves the unfolded protein response (UPR) including activation of the IRE1α-XBP1 pathway. In addition, MM cells are located in the bone marrow milieu, which is usually considered hypoxic compared with other organs.[9,10] Therefore, MM cells have to survive and grow even at low oxygen, with poor nutrition and adverse pH *in vivo*. Thus, MM cells need to possess mechanisms to protect against ER stress. Among the UPR in MM cells, the IRE1α-XBP1 pathway has been implicated in the proliferation and survival of MM cells to a greater extent than in monoclonal gammopathy of undetermined significance or normal plasma cells.[11] It has been reported to be a prognostic factor[12] and could be a target for immunotherapy[13] or chemotherapy.[14] Based on previous reports, it is proposed that an inhibitor of IRE1α-XBP1 activation should be a potent therapeutic agent for MM.

The transcriptional activity of XBP1 is regulated by ER-located transmembrane kinase/endoribonuclease (RNase) protein IRE1α. Recent studies have proposed a model of ER stress-induced IRE1α activation and subsequent XBP1 activation as follows: (1) accumulation of unfolded proteins triggers oligomerization of luminal domains of IRE1α.[15] (2) Oligomerization of IRE1α causes trans-auto-phosphorylation of the kinase activation loop domain, which leads to a conformational change.[16–19] (3) This conformational change permits cofactor (ADP) binding,[16,20] promoting back-to-back dimer configuration of cytosolic domains.[21] (4) The oligomerization of cytosolic domains activates the RNase activity of IRE1α which subsequently cleaves XBP1 mRNA at two sites to initiate an unconventional splicing reaction.[21] (5) IRE1α-induced cleavage of XBP1 mRNA results in the removal of a 26-nucleotide intron and the 5′ and 3′ fragments are subsequently joined by RNA ligase activity.

[1]Department of Medical Oncology and Immunology, Nagoya City University Graduate School of Medical Sciences, Nagoya, Japan; [2]Department of Bioscience and Informatics, Faculty of Science and Technology, Keio University, Yokohama, Japan; [3]Iwawaki Laboratory, Advanced Scientific Research Leaders Development Unit, Gunma University, Maebashi, Japan and [4]Fuji Research Park, Kyowa Hakko Kirin Co., Ltd., Shizuoka, Japan. Correspondence: Dr S Iida, Department of Medical Oncology and Immunology, Nagoya City University Graduate School of Medical Sciences, 1 Kawasumi, Mizuho-chou, Mizuho-ku, Nagoya, Aichi 467-8601, Japan.
E-mail: iida@med.nagoya-cu.ac.jp
[5]These authors contributed equally to this work.
Received 26 March 2012; revised 19 June 2012; accepted 22 June 2012

This unconventional splicing reaction creates a translational frame shift to produce an active XBP1 transcription factor.[22,23]

Previously, we reported a novel screening system for inhibitors of XBP1 activation, using luciferase reporter signals in HeLa/XBP1-luc cells.[24] In the present study, we identified toyocamycin[25] as an XBP1 inhibitor in the culture broth of an *Actinomycete* strain using this screening system (Figure 1a). We observed that toyocamycin inhibited IRE1α-induced ATP-dependent XBP1 mRNA cleavage *in vitro* without affecting IRE1α auto-phosphorylation. Moreover, this compound markedly inhibited not only ER stress-induced but also constitutively activated IRE1α-XBP1 pathway both in MM cell lines and primary MM cells, resulting in strong cytotoxic activity.

MATERIALS AND METHODS

Cell culture and reagents

Human epithelial adenocarcinoma HeLa cells and previously generated HeLa/XBP1-luc cells[24] were cultured in DMEM supplemented with 10% FBS. Human MM and other hematological cell lines were cultured in RPMI-1640 supplemented with 10% FBS. Human fibrosarcoma HT1080 was cultured in EMEM supplemented with 2 mM glutamine, 1% non-essential amino acids and 10% FBS. A BTZ-resistant MM cell lines, KMS-11/BTZ and OPM-2/BTZ, were established from the parental line, KMS-11 and OPM-2, respectively, under continuous exposure to BTZ over a half year.[26] Toyocamycin, sangivamycin, tubercidin, tunicamycin, 2-deoxyglucose and 5-fluorouracil were purchased from Sigma-Aldrich (St Louis, MO, USA). Thapsigargin was purchased from Santa Cruz Biotechnology (Santa Cruz, CA, USA). BTZ was purchased from Toronto Research Chemicals (North York, ON, Canada).

Primary MM specimens

Nine primary MM specimens derived from eight patients with symptomatic MM were obtained after written informed consent at Nagoya City University Hospital. The assay protocols using patient samples were approved by the Institutional Ethical Committee. MM cells were purified from the marrow mononuclear cell fraction or pleural effusion using

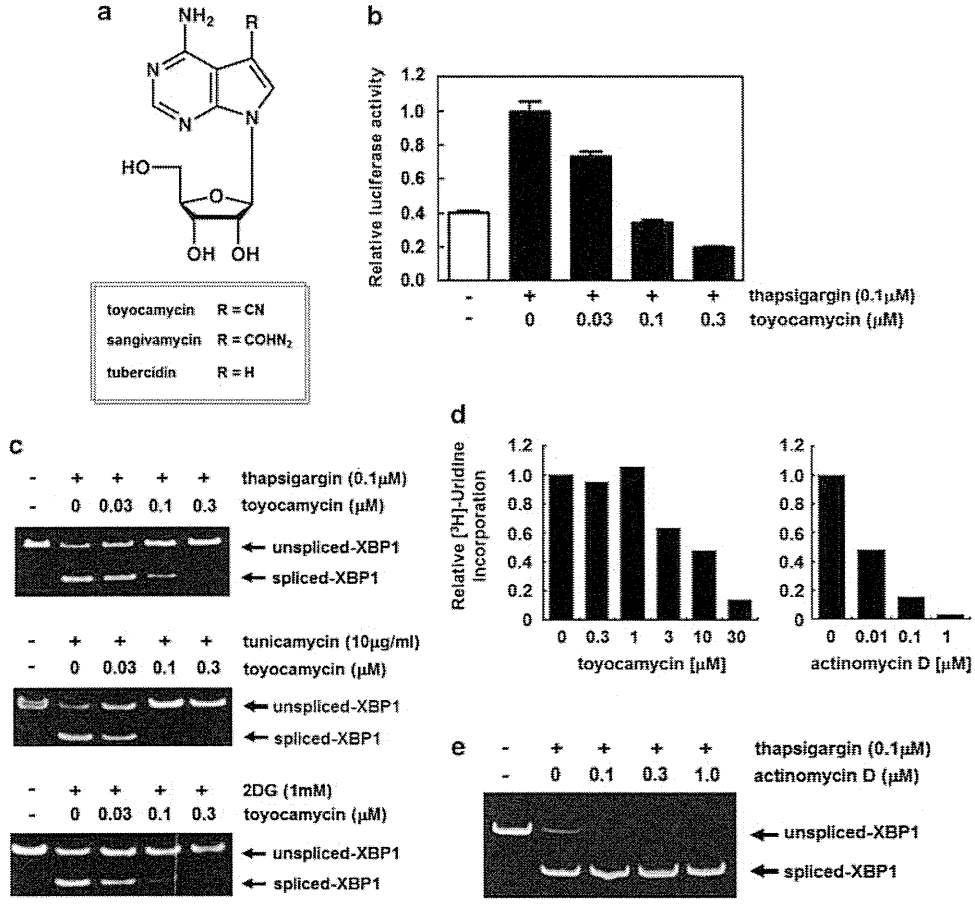

Figure 1. Toyocamycin suppressed thapsigargin, tunicamycin or 2-deoxyglucose-induced XBP1 mRNA splicing. (**a**) Structure of toyocamycin, sagivamycin and tubercidin. (**b**) Effect of toyocamycin on thapsigargin-induced XBP1 activation. HeLa/XBP1-luc cells were treated with the indicated concentration of toyocamycin in the presence of 0.1 μM of thapsigargin. After 24 h, the cells were lysed and subjected to luciferase assay. Data are the fold change + s.d. of a thapsigargin-induced luciferase activity in the presence or absence of various concentration of toyocamycin. All experiments were performed in triplicate. (**c**) Toyocamycin inhibition of thapsigargin-, tunicamycin- or 2-deoxyglucose (2DG)-induced endogenous XBP1 mRNA splicing. HeLa cells were treated with the indicated concentration of toyocamycin in the presence or absence of 0.1 μM of thapsigargin, 10 μg/ml of tunicamycin or 1 mM of 2DG for 4 h. The cells were collected and RNA extracted. Spliced- or unspliced-XBP1 mRNA was detected as described in Materials and methods. (**d**) Effect of toyocamycin or actinomycin D on [^{3}H]-uridine incorporation into acid-insoluble fractions of HeLa cells. HeLa cells were incubated with the indicated concentration of toyocamycin or actinomycin D in the presence of 1 μCi/ml [^{3}H]-uridine for 1 h. The reaction was stopped by addition of 10% TCA, and the acid-insoluble fractions were collected. Data represent the mean of three experiments. (**e**) Effect of actinomycin D on thapsigargin-induced endogenous XBP1 mRNA splicing assessed by RT-PCR. HeLa cells were treated with the indicated concentration of actinomycin D in the presence or absence of 0.1 μM of thapsigargin for 4 h. The cells were collected and RNA extracted. Spliced- or unspliced-XBP1 mRNA was detected as described in Materials and Methods.

anti-CD138 antibody-coated beads with the aid of an automatic magnetic cell sorting system (Miltenyi Biotec, Auburn, CA, USA).[26]

Preparation of toyocamycin

The culture broth (3 l) of *Streptmyces* sp. 1893-56 was extracted with EtOAc, filtered and concentrated *in vacuo*. This suspension was extracted with hexane, and the insoluble fraction concentrated. The active fractions were then collected and further isolated by silica gel column chromatography (Silica gel 60, 60–230 μm; Merck, Darmstadt, Germany) using a $CHCl_3$-MeOH stepwise system. As a result, we obtained 5 mg of active compound. The UV spectrum, HRESI-MS measurement, and ^1H NMR spectra of this active compound confirmed its identity as toyocamycin.

Luciferase assay

As previously reported,[24] HeLa/XBP1-luc cells were seeded into 96-well plates at 2×10^4 cells/well, and then incubated with 0.1 μM of thapsigargin together with or without test compounds. After 24 h of incubation, the cells were lysed in Passive lysis buffer (Promega, Madison, WI, USA), and luciferase activity measured using the luciferase assay system (Promega) and a luminometer (Wallac, PerkinElmer, Waltham, MA, USA). IC_{50} values were determined from the dose–response curves of the inhibition of XBP1-luciferase activity, setting the result of thapsigargin treatment as 100%.

Reverse transcriptase (RT)-PCR and real-time PCR analysis

HeLa cells and MM cell lines were incubated with test compounds for 4 or 6 h together with the ER stress inducers thapsigargin, tunicamycin, or 2-deoxyglucose. Briefly, total RNA was extracted from HeLa cells using TRIzol reagent (Invitrogen, Carlsbad, CA, USA). Aliquots of 2 μg of total RNA were treated with M-MLV reverse transcriptase (Promega) to produce first-strand complementary DNA (cDNA). For RT-PCR analysis, this first-strand cDNA was subjected to PCR with KOD plus polymerase (Toyobo, Osaka, Japan) using a pair of primers corresponding to nucleotides 505–525 and 609–629 of XBP1 cDNA. The amplified products were separated by electrophoresis on an 8% polyacrylamide gel and visualized by ethidium bromide staining.

For real-time RT-PCR analysis, the synthesized first-strand cDNA was amplified in triplicate using SYBR Premix ExTaq (TaKaBaBio, Shiga, Japan), and the products were detected on a MiniOpticon system (Bio-Rad, San Diego, CA, USA). PCRs were incubated for 10 s at 95 °C followed by 45 amplification cycles with 3 s denaturing at 95 °C, 10 s annealing at 60 °C and 10 s extension at 72 °C. The primers designed for quantitative real-time RT-PCR analysis were as follows: for GRP78, 5′-GCGCATGAAGGAGAAAGAAC-3′ and 5′-TCACCATTCGGTCAATCAGA-3′; for ERdj4, 5′-AAAATAAGAGCCCGGATGCT-3′ and 5′-CGCTTCTTGGATCCAGTGTT-3′; for EDEM, 5′-TGGACTGCAGGTGCTGATAG-3′ and 5′-GGATTCTTGGTTGCCTGGTA-3′; and for GAPDH, 5′-AGGTCGGAGTCAACGGATTT-3′ and 5′-TAGTTGAGGTCAATGAAGGG-3′. Specificity of the PCR was evaluated by analyzing melting curves and sequences of the amplicons.

For the detection of spliced XBP1 isoform or all forms (spliced and unspliced), primer sets and Taqman probes were purchased from Applied Biosystems (Foster City, CA, USA). Quantitative PCR was performed using Taqman Gene Expression Assays and a StepOnePlus real-time PCR instrument according to the manufacturer's instructions.

Western blotting

Western blotting was performed as described.[27] Primary antibodies used were: anti-KDEL from Enzo LifeScience (Farmingdale, NY, USA); anti-ATF6, anti-actin and anti-XBP1 from Santa Cruz Biotechnology; anti-phospho-eIF2α (Ser51) and anti-eIF2α and anti-IRE1α from Cell Signaling (Boston, MA, USA); anti-tubulin and anti-FLAG (M2) from Sigma (St Louis, MO, USA); anti-phospho-Ser724-IRE1α from Novus Biologicals (Littleton, CO, USA).

In vitro XBP1 mRNA cleavage assay

In vitro XBP1 mRNA cleavage assays were performed as described previously.[28] Briefly, 337-nucleotide RNA substrate (XBP1(266-602) RNA) consisting of the XBP1 intron (26 nucleotides) flanked on both sides by truncated exon sequences (228 nucleotides on the 5′ side and 83 nucleotides on the 3′ side), which contained the minimum sequence for ER stress-induced XBP1 splicing, was prepared by *in vitro* transcription using T7 RNA polymerase. N-terminally FLAG-tagged human IRE1α(467-977) was prepared by immunoprecipitation with anti-FLAG antibody from 293T cells transiently transfected with pCAX-FLAG-IRE1α(467-977) plasmid. The IRE1α(467-977)-induced XBP1(206-602) mRNA cleavage reaction was performed in the presence of 100 μM ATP. RNA fragments were resolved on a 7 M urea 6% PAGE gel and stained with ethidium bromide.

Apoptosis and cell proliferation assays

After exposure to toyocamycin or BTZ, apoptotic cells were evaluated using the Annexin V-FITC Apoptosis Detection Kit I (BD Pharmingen, Franklin Lakes, NJ, USA). The cell proliferation assay has been described previously.[26] The percentage of specific apoptosis was calculated as follows: % specific apoptosis = (% AnnexinV-positive cells − % spontaneous AnnexinV-positive cells)/(100 − % spontaneous positive cells) × 100.

Cell proliferation assays of the MM cell lines, primary MM cells from patients and peripheral blood mononuclear cell (PBMC) from healthy individuals exposed to various concentrations of toyocamycin for 24 h were performed using the CEllTiter 96 AQueous One Solution Cell Proliferation Assay Kit (Promega) as described previously.[26] The mean of three determinations at each concentration of BTZ was calculated, and IC_{50} values were obtained using XLfit 4.2 curve fitting software for Excel (ID Business Solutions Inc., Alameda, CA, USA).

Animals and the murine xenograft model

Animal studies were performed in conformity with the UK Coordinating Committee on Cancer Research Guidelines for the Welfare of Animals in Experimental Neoplasia (second edition). The study method was described previously.[29] Briefly, 0.5×10^7 RPMI8226 cells were inoculated subcutaneously into SCID mice previously administered with rabbit antiasialo-GM1 intraperitoneally (Wako Pure Chemical Industries, Osaka, Japan) 1 day before tumor inoculation. At 10 days after tumor inoculation, the tumor-bearing mice were divided into four groups of five mice each, such that the mean tumor volumes were approximately equal in the four groups. Tumor volume was calculated by the following formula: tumor volume $(mm^3) = 0.5 \times (\text{major diameter}) \times (\text{minor diameter})^2$. Mice were treated by intraperitoneal injection of 0.5 mg/kg toyocamycin twice weekly, 1.0 mg/kg toyocamycin once weekly, or 1.0 mg/kg BTZ twice weekly for 2 weeks. Volumes of tumors in toyocamycin-treated mice were compared with untreated or BTZ-treated animals during the treatment period.

Statistical analysis

The significance of differences in tumor volume between toyocamycin-treated mice and others were examined with the Mann–Whitney *U*-test. Data were analyzed with the aid of StatView software ver. 5.0 (SAS Institute, Cary, NC, USA). In this study, $P < 0.05$ was considered significant.

RESULTS

Identification of toyocamycin as an inhibitor of ER stress-induced XBP1 mRNA splicing

Previously, we established a screening system for inhibitors of ER stress-induced XBP1 activation and identified the new active small molecules trierixin and quinotrierixin.[24,30] In the course of further screening for an inhibitor of ER stress-induced XBP1 activation, we isolated toyocamycin[25] from a culture broth of an *Actinomycete* strain (Figure 1a). As shown in Figure 1b, 0.1 μM thapsigargin, an inhibitor of the ER calcium pump (SERCA), elevated XBP1-luciferase activity about 2.5-fold more than the control in HeLa/XBP1-luc cells. Toyocamycin suppressed thapsigargin-induced XBP1-luciferase activation in a dose-dependent manner with an IC_{50} value of 0.08 μM. To examine whether toyocamycin also inhibited thapsigargin-induced endogenous XBP1 mRNA splicing in HeLa cells, we next performed RT-PCR analysis of RNA isolated from toyocamycin-treated or -untreated HeLa cells. As shown in Figure 1c, toyocamycin suppressed thapsigargin-induced XBP1 mRNA splicing in a dose-dependent manner with an IC_{50} value of 0.18 μM. Furthermore, toyocamycin also suppressed tunicamycin, a N-glycosylation inhibitor, or 2-deoxyglucose, a

hypoglycemia-mimicking agent, -induced XBP1 mRNA splicing with an IC_{50} value of 0.13 μM and 0.11 μM, respectively (Figure 1c). These results show that toyocamycin inhibits ER stress-induced XBP1 mRNA splicing.

The inhibitory activity of toyocamycin on RNA synthesis is not responsible for inhibition of ER stress-induced XBP1 mRNA splicing

Because previous studies have reported that toyocamycin inhibits RNA synthesis in mammalian cells,[31,32] we tested whether its inhibitory activity on ER stress-induced XBP1 mRNA splicing was due to the inhibition of RNA synthesis. As shown in Figure 1d, toyocamycin suppressed incorporation of [^{3}H]-uridine into the macromolecular fraction of HeLa cells in a dose-dependent manner with an IC_{50} value of 12 μM without affecting incorporation of [^{3}H]-thymidine or [^{3}H]-leucine. This indicates that toyocamycin inhibits RNA synthesis in HeLa cells. However, the IC_{50} value of toyocamycin for RNA synthesis is much higher than for ER stress-induced XBP1 mRNA splicing. On the other hand, actinomycin D, a well-known RNA synthesis inhibitor, also blocked the incorporation of [^{3}H]-uridine into HeLa cells in a dose-dependent manner with an IC_{50} value of 0.06 μM. However, as shown in Figure 1e, actinomycin D did not suppress thapsigargin-induced XBP1 mRNA splicing even at 0.1 μM (which caused 80% inhibition of RNA synthesis). These results indicate that actinomycin D does not inhibit ER stress-induced XBP1 mRNA splicing. Therefore, we conclude that the inhibitory activity of toyocamycin on ER stress-induced XBP1 mRNA splicing is not due to the inhibition of RNA synthesis.

The adenosine moiety of toyocamycin is important for inhibition of XBP1 mRNA splicing

We next investigated whether sangivamycin or tubercidin, a small molecule structurally related to toyocamycin (Figure 1a), also inhibited ER stress-induced XBP1 activation. As shown in Table 1, sangivamycin and tubercidin inhibited thapsigargin-induced XBP1-luciferase activation in a dose-dependent manner with IC_{50} values of 0.5 and 0.34 μM, respectively. Furthermore, sangivamycin and tubercidin also inhibited thapsigargin-induced endogenous XBP1 mRNA splicing evaluated by RT-PCR analysis (data not shown). On the other hand, 5-Aza-2-deoxycytidine (5Aza-C), a cytidine analog, or 5-fluorouridine, a uridine analog, neither inhibited thapsigargin-induced XBP1-luciferase activation nor endogenous XBP1 mRNA splicing even at 100 μM (Table 1 and data not shown). These results suggest that the adenine moiety of toyocamycin is important for inhibition of XBP1 activation.

Toyocamycin selectively inhibits the IRE1α-XBP1 pathway

We next examined the effect of toyocamycin on the transcriptional activity of XBP1. Consistent with the regulation of transcription of EDEM and ERdj4 by the IRE1-XBP1 pathway,[33,34] toyocamycin suppressed tunicamycin-increased EDEM and ERdj4 mRNA with an IC_{50} of 0.079 and 0.172 μM, respectively (Figure 2a). These results suggest that toyocamycin might be inhibiting the transcriptional activity of XBP1 due to inhibition of ER stress-induced XBP1 mRNA splicing. On the other hand, because ER stress activates the three ER transmembrane proteins, IRE1, ATF6 and PERK, we also investigated whether toyocamycin inhibited ER stress-induced activation of ATF6 and PERK. ATF6 is constitutively synthesized as a type-II transmembrane protein in the ER.[35] This membrane-bounded precursor form, designated as pATF6(P), is transported to the Golgi apparatus in response to ER stress, where it is cleaved by the sequential actions of Site-1 and Site-2 proteases.[36–39] The cytoplasmic region of ATF6 thus liberated from the membrane is translocated into the nucleus, where it functions as an active transcription factor. PERK is a serine–threonine protein kinase that phosphorylates eukaryotic initiation factor-2α (eIF2α) on Ser51.[40,41] Therefore, we assessed ATF6 activation and PERK activation by measuring the amount of the precursor form of ATF6 (pATF6(P)) and the phosphorylation of eIF2α on Ser51, respectively. As shown in Figure 2b, tunicamycin decreased the 90 kDa membrane-bound precursor form of ATF6 (pATF6(P)) and phosphorylated eIF2α on Ser51, indicating that it activated both ATF6 and PERK. However, toyocamycin inhibited neither the tunicamycin-induced decrease of pATF6(P) nor phosphorylation of eIF2α on Ser51. These results indicate that toyocamycin selectively inhibits the ER stress-induced activation of the IRE1α-XBP1 pathway.

Table 1. The IC_{50} of inhibition of XBP1-luciferase activation when exposed to each drug

Small-molecule inhibitor	*XBP1-luciferase inhibition (μM)*
Toyocamycin	0.08
Sangivamycin	0.5
Tubecidin	0.34
5-aza-2-deoxycytidine	>100
5-fluoro-uridine	>100

IC_{50} values were determined from the dose–response curves of the inhibition of XBP1-luciferase activity.

Toyocamycin inhibits IRE1α-induced XBP1 mRNA cleavage

We next investigated the mechanism by which toyocamycin inhibits ER stress-induced activation of the IRE1α-XBP1 pathway. Overexpression of IRE1α has been reported to lead to IRE1α homo-oligomerization, which occurs without accumulation of unfolded proteins in the ER or GRP78 dissociation from IRE1α.[42,43] Indeed, as shown in Figure 2c, overexpression of IRE1α induced Ser724 phosphorylation and XBP1 mRNA splicing even under normal conditions in 293T cells transiently transfected with pcDNA3-IRE1α-FLAG plasmid. Although toyocamycin did not affect the Ser724 phosphorylation of IRE1α, it inhibited IRE1α overexpression-induced XBP1 mRNA splicing in a dose-dependent manner. On the other hand, toyocamycin inhibited IRE1α (467-977)-induced XBP1 mRNA cleavage *in vitro* (Figure 2d). Thus, these results indicate that toyocamycin inhibits IRE1α-induced XBP1 mRNA cleavage.

Toyocamycin inhibits constitutive activation of XBP1 in MM cell lines

As shown in Figure 3a, most MM cell lines have activated XBP1 protein expression, represented as the overexpression of spliced XBP1 isoform, whereas non-MM cells including other hematological malignant and solid tumor cells have little activation of XBP1. This suggests that the IRE1α-XBP1 pathway is constitutively active in MM cells but not in non-MM cells. Among 10 MM cell lines, 7 MM cells including FR4, RPMI8226, XG7, OPM-2, ILKM2, ILKM8 and AMO1 express high levels of spliced-XBP1, whereas other 3 including U266, KMS-11 and SKMM1 express relatively lower levels.

We next tested the influence of toyocamycin on the constitutive activation of XBP1 in MM cell lines. After treatment with 10 nM or higher concentrations of toyocamycin, the levels of spliced isoform of XBP1 protein in RPMI8226 cells declined and resulted in caspase activation (Figure 3b). The level of spliced-XBP1 mRNA in RPMI8226 cells decreased at 6 h after exposure to 100 nM toyocamycin (Figure 3c). The protein levels of spliced-XBP1 also decreased by toyocamycin treatment, whereas phosphorylated levels of IRE1α remained unchanged. A similar reduction in the levels of spliced-XBP1 following toyocamycin treatment was also confirmed in two other MM cell lines, such as XG7 and U266, harboring high or low active XBP1 expression at baseline, respectively (Figure 3d). Furthermore, toyocamycin inhibited thapsigargin-induced expression of spliced XBP1 protein without affecting IRE1α phosphorylation on Ser724 (Supplementary Figure 3).

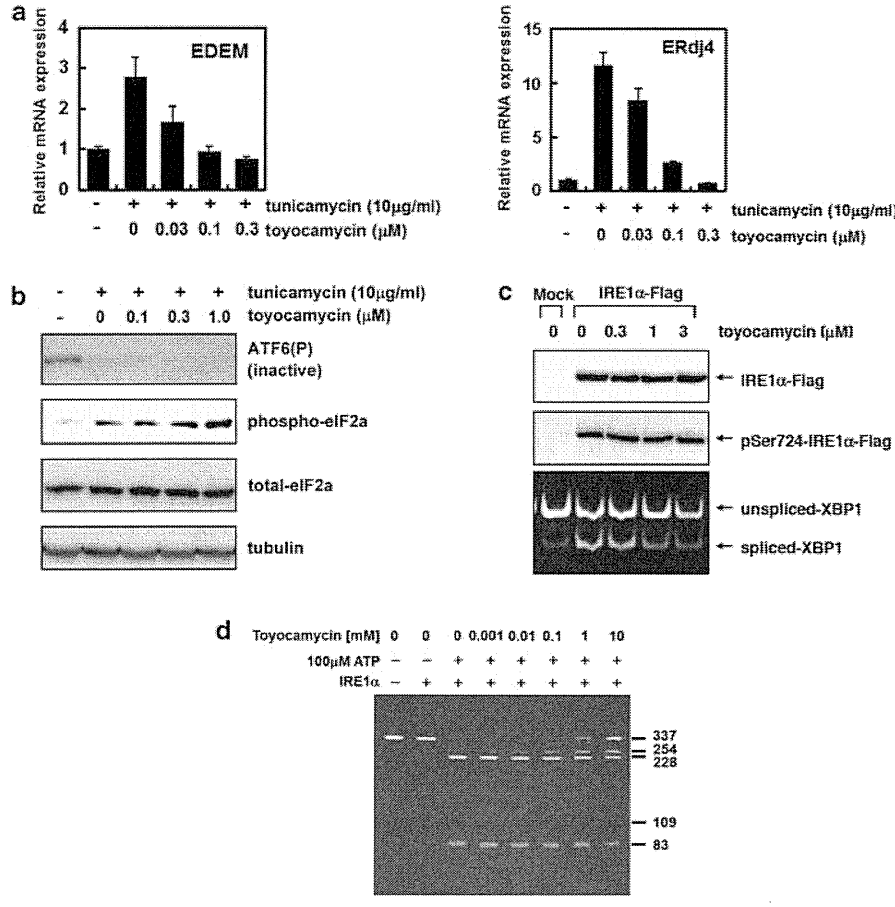

Figure 2. Toyocamycin selectively inhibits ER stress-induced activation of the IRE1α-XBP1 pathway and IRE1α-induced XBP1 mRNA cleavage. (**a**) Toyocamycin suppresses tunicamycin-induced EDEM and ERdj4 mRNA expression in HeLa cells. HeLa cells were incubated with the indicated concentration of toyocamycin in the presence or absence of 10 μg/ml tunicamycin for 4 h. Thereafter, the cells were collected and expression of EDEM and ERdj4 mRNA quantified by real-time RT-PCR as described in Materials and methods. Data represent the mean ± s.d. of three experiments. (**b**) Toyocamycin suppresses neither tunicamycin-induced ATF6 nor PERK activation. HeLa cells were treated with the indicated concentration of toyocamycin in the presence or absence of 10 μg/ml of tunicamycin for 4 h. Thereafter, cells were collected and subjected to western blotting using anti-ATF6, anti-phospho-eIF2α, anti-eIF2α or anti-tubulin antibody. (**c**) Toyocamycin does not inhibit IRE1α phosphorylation on Ser724. HEK293T cells were transiently transfected with 1 μg of pcDNA3-IRE1α-flag plasmid. After 24 h, the cells were treated with the indicated concentration of toyocamycin for 4 h. The cells were collected and subjected to western blotting using anti-FLAG, anti-Ser724-IRE1α antibodies. Another set of the cells was collected and RNA was extracted. Spliced- or unspliced-XBP1 mRNA was detected as described in Materials and Methods. (**d**) Toyocamycin inhibits IRE1α-induced XBP1 mRNA cleavage *in vitro*. A 337-nucleotide RNA substrate (XBP1 (266-602) RNA) containing the XBP1 intron (26 nucleotides) was mixed with N-terminally FLAG-tagged human IRE1α(467-977) in the presence of 100 μM of ATP. RNA fragments were resolved on a 7 M urea 6% PAGE gel and stained with ethidium bromide.

Toyocamycin induces marked apoptosis of MM cell lines harboring high levels of spliced-XBP1

Two MM cell lines with highly expressed spliced-XBP1, including RPMI8226 and XG7, showed robust dose-dependent apoptosis after exposure to various concentrations of toyocamycin for 24 h, as assessed by the number of Annexin V-positive cells (Figure 3e). These cells showed marked apoptosis at 30 nM or higher concentrations of toyocamycin, whereas U266 cells with relatively low spliced-XBP1 expression showed mild apoptosis compared with that of RPMI8226 and XG7.

MM cells with high spliced-XBP1 expression show marked growth inhibition compared with those with low spliced-XBP1 expression and to non-MM cells by toyocamycin treatment

We then evaluated the growth inhibitory effect of toyocamycin on seven MM cell lines with high spliced-XBP1 expression, three MM cell lines with low spliced-XBP1 expression and four non-MM cell lines. All MM cells with high spliced-XBP1 expression showed remarkable decline in cellular viability at 30 nM or higher concentrations of toyocamycin (Figure 4a, left) than the other MM cells with low spliced-XBP1 expression (Figure 4a, middle). Most non-MM cells showed the subtle reduction in cellular viability even at the higher concentrations of toyocamycin (Figure 4a, right). The mean IC_{50} values of toyocamycin on two MM cell groups, each having high or low spliced-XBP1 expression were 17.69 ± 2.78 and 88.57 ± 38.31 nM, respectively, and this difference was considered statistically significant ($P = 0.016$) (Figure 4b).

Toyocamycin also induces marked apoptosis on BTZ-resistant MM cells

Two BTZ-resistant MM cell lines, KMS-11/BTZ and OPM-2/BTZ showed a little apoptosis progression even in the presence of 10 or 30 nM of BTZ, at which most MM cell lines including parental cells of these resistant ones were induced to marked apoptosis. However, they showed remarkable apoptosis in the presence of 30 or 100 nM of toyocamycin (Figure 4c).

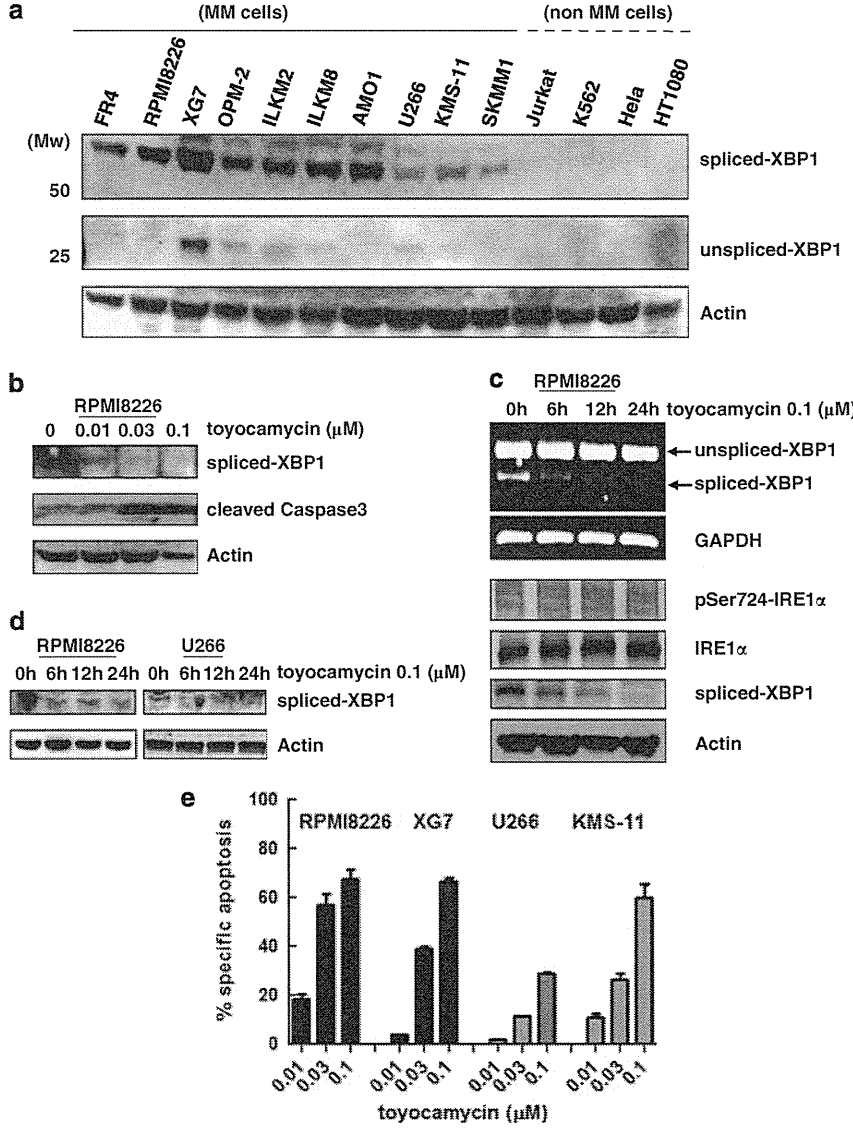

Figure 3. Toyocamycin inhibits constitutive activation of XBP1 in MM cells, and triggers marked apoptosis of MM cell lines. (**a**) XBP1 expression consisting of spliced and unspliced form was assessed by immunoblot analysis in 10 MM and 4 non-MM cell lines including 2 of hematological and 2 of solid tumor origin. (**b**) Reduced expression of spliced XBP1 isoform induced by various concentrations of toyocamycin in RMPI8226 cells detected by immunoblot. (**c**) RPMI8226 cells were treated with 0.1 μM of toyocamycin and the altered expression of IRE1α-XBP1 were evaluated by RT-PCR and immunoblot analysis. (**d**) The kinetic change of constitutive XBP1 expression in two MM cell lines during exposure to 0.1 μM toyocamycin. (**e**) Toyocamycin induced apoptosis in three MM cell lines, RPMI8226, XG7 and U266. Cells were treated with toyocamycin at the indicated concentration for 24 h and apoptotic cells were evaluated by double staining with Annexin V and PI. Data represent the mean + s.d. of three independent experiments.

Toyocamycin cooperates with BTZ to mediate anti-tumor effects on MM cells

At suboptimal concentrations toyocamycin mediated a little apoptosis induction (Figure 3e) in MM cells. However, treatment with 5 or 10 nM toyocamycin together with 6 nM BTZ-mediated additive or synergistic cytotoxicity in RPMI8226 cells (Figure 4d).

Toyocamycin is also cytotoxic for primary MM cells, associated with inhibition of IRE1α-XBP1 activation

Most freshly prepared primary MM cells had activated XBP1 expression, represented as a high ratio of XBP1-spliced isoform: all isoforms (1.74:3.43; median 2.48), although the mRNA levels are similar to those in healthy donor control PBMC (Figure 5a). The relative amount of spliced-XBP1 mRNA in five MM samples (#2, #4, #5, #8 and #9), which was quantitated by real-time PCR method, decreased after 6 h exposure to toyocamycin (Figure 5b). Most of the primary MM cells were sensitive to 10 nM BTZ (17.1–106.8; median 48.8) and they also showed dose-dependent reduced viability following toyocamycin treatment (Figure 5c). Of nine MM samples, sample no. 4 was derived from the pleural effusion of a patient with MM refractory to BTZ; these tumor cells were resistant to BTZ *in vitro*. Nonetheless, toyocamycin was also cytotoxic for these cells (Supplementary Figure 4). In contrast, toyocamycin showed little cytotoxicity against healthy PBMC even at higher concentrations for 24 h (Figure 5d). Three primary MM samples (#5, #8 and #9) with sufficient cell numbers for protein analysis, showed reduction in activated (spliced) XBP1 protein after 6 h treatment with toyocamycin (Figure 5e). As in the MM cell lines, the phosphorylation status of IRE1α was not affected by toyocamycin.

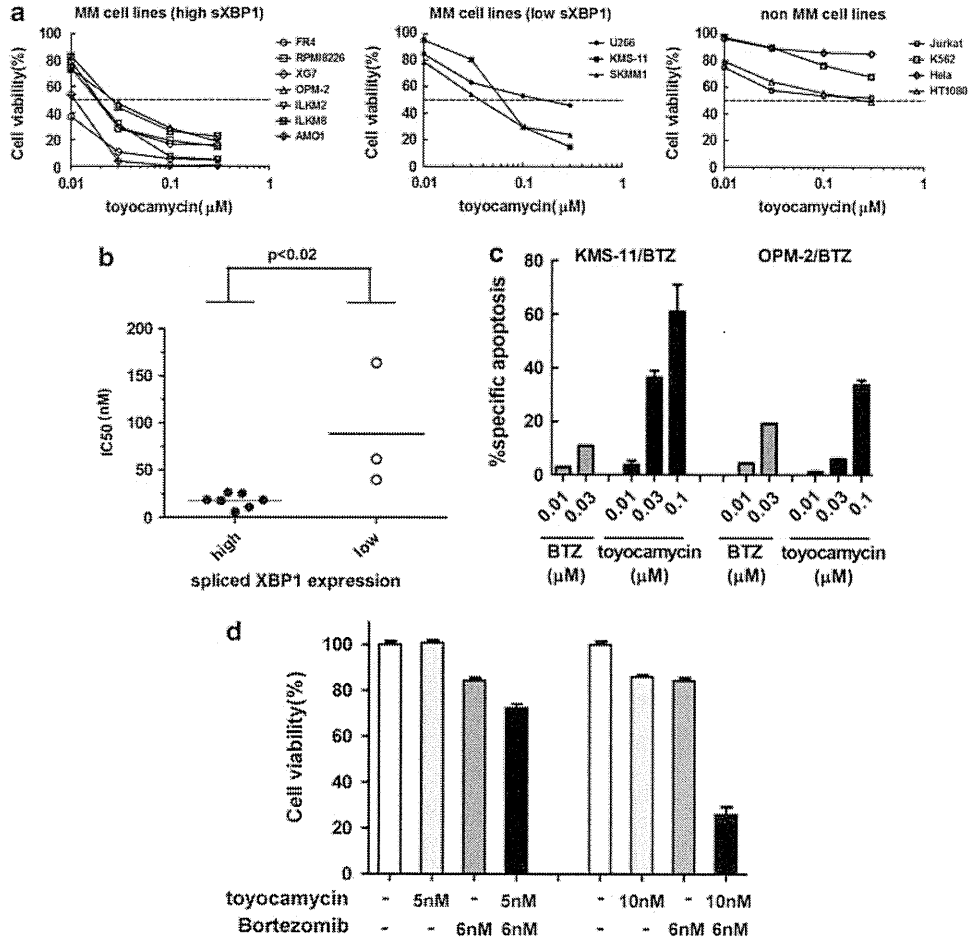

Figure 4. Growth inhibitory effect of toyocamycin on MM cells with high or low expression of spliced XBP1 and on non-MM cells. (**a**) Growth inhibitory effect of toyocamycin exposure for 24 h on two groups of MM cells with high or low expression of spliced XBP1 and on non-MM cells. Data represent the mean of three independent experiments. (**b**) The IC_{50} values of each MM cell line after 24 h exposure to toyocamycin are calculated and plotted according to the high or low expression of XBP1. (**c**) Toyocamycin induced marked apoptosis of the BTZ-resistant MM cell lines, KMS-11/BTZ and OPM-2/BTZ. These two MM cells were treated, respectively, with BTZ or toyocamycin alone at the indicated concentrations for 24 h. Each column represents the mean + s.d. of three independent experiments. (**d**) RPMI8226 cells were exposed to either 5 or 10 nM of toyocamycin in the presence or absence of bortezomib (6 nM) for 72 h. Cell viability was measured by MTS assay. Data represent the mean ± s.d. of three independent experiments.

In vivo anti-tumor activity of toyocamycin alone and in combination with BTZ in a human MM xenograft model

To evaluate *in vivo* efficacy of toyocamycin on MM cells, SCID mice subcutaneously inoculated with RPMI8226 were treated with twice- or once-weekly intraperitoneal toyocamycin at either 0.5 or 1.0 mg/kg. In addition, the combination treatment of toyocamycin with BTZ was tested. Toyocamycin alone showed robust anti-tumor activity resulting in smaller tumor volumes compared with controls on day 15. This was similar to the effect of BTZ (Figures 6a and b). No obvious difference in tumor inhibitory effect was seen on twice- or once-weekly injection of toyocamycin.

The combination treatment of BTZ with toyocamycin, either at 0.5 mg/kg or 1.0 mg/kg, showed a trend toward enhancing anti-tumor activity represented as smaller tumor volumes when compared with BTZ or toyocamycin alone (Figures 6a and b).

DISCUSSION

Several lines of evidence suggest the importance of the IRE1α-XBP1 pathway in tumor progression, adaptation to the hypoxic tumor microenvironment, as a prognostic marker and a potential therapeutic target in both solid tumors and MM. Here, we identified toyocamycin as an inhibitor of both ER stress-induced and constitutive activation of the IRE1α-XBP1 pathway in MM cells, and showed that it exerted synergistic or at least additive anti-tumor effects with BTZ. Furthermore, it induced marked apoptosis of primary MM cells as well as MM cell lines without showing any cytotoxicity to PBMCs from healthy donors. This anti-tumor effect was also confirmed in a mouse model *in vivo*.

Previously, toyocamycin was reported to inhibit RNA synthesis and ribozyme function.[31,32,44] This raised the possibility that it inhibited ER stress-induced XBP1 mRNA splicing and transcription of *EDEM* and *ERdj4* genes through RNA synthesis inhibition. However, comparing the IC_{50} values of toyocamycin on RNA synthesis, ER stress-induced XBP1 mRNA splicing and transcription of UPR target genes revealed that its inhibitory activity on ER stress-induced XBP1 mRNA splicing and transcription of *EDEM* and *ERdj4* genes was much stronger than the RNA synthesis blockade effect. Furthermore, although 100 nM actinomycin D completely inhibited both RNA synthesis (Figure 1d) and ER stress-induced transcription of GRP78 (Supplementary Figure 1), it did not inhibit ER stress-induced XBP1 mRNA splicing (Figure 2b). These results support the notion that the inhibitory activity of toyocamycin on RNA synthesis is not responsible for inhibition of XBP1 mRNA splicing and transcription of *EDEM* and *ERdj4* genes. On the other hand, toyocamycin has also been reported to inhibit kinase